PREPARATION, CHARACTERIZATION AND ACTIVITY EVALUATION OF MULTI-COMPONENT PHOTOCATALYST UNDER VISIBLE LIGHT IRRADIATION

NOR AMALINA BINTI HUSSAIN

BACHELOR OF CHEMICAL ENGINEERING

UNIVERSITI MALAYSIA PAHANG

PREPARATION, CHARACTERIZATION AND ACTIVITY EVALUATION OF MULTI-COMPONENT PHOTOCATALYST UNDER VISIBLE LIGHT IRRADIATION

NOR AMALINA BINTI HUSSAIN

UNIVERSITI MALAYSIA PAHANG

PREPARATION, CHARACTERIZATION AND ACTIVITY EVALUATION OF MULTI-COMPONENT PHOTOCATALYST UNDER VISIBLE LIGHT IRRADIATION

NOR AMALINA BINTI HUSSAIN

Thesis submitted in fulfillment of the requirements
for the award of the degree of
Bachelor of Chemical Engineering

Faculty of the Chemical Engineering and Natural Resources
UNIVERSITI MALAYSIA PAHANG

JANUARY 2012

SUPERVISOR'S DECLARATION

We hereby declare that we have checked this project report and in our opinion this project is satisfactory in terms of scope and quality for the award of the degree of Bachelor of Chemical Engineering.

Signature : .....

Name of Supervisor : MD MAKSUDUR RAHMAN KHAN

Position : ASSOCIATE PROFESSOR

Date : 20th JANUARY 2012

STUDENT'S DECLARATION

I hereby declare that the work in this report is my own except for quotations and summaries which have been duly acknowledged. The report has not been accepted for any degree and is not concurrently submitted for award of other degree.

Signature : …….....
Name : NOR AMALINA BINTI HUSSAIN
ID Number : KA08083
Date : 20th JANUARY 2012

Special dedication

To my lovely family and my beloved husband, Ahmad Asnawi bin Alias who offered me unconditional love and support throughout the course of this thesis

ACKNOWLEDGEMENT

Firstly, I am thankful to ALLAH S.W.T for blessing me in completing thesis for final year project (FYP) with successful and achieved the objectives of this project. Hopefully, this research about wastewater treatment will be benefit to people in the future.

In this opportunity, I would like to give my sincere gratitude to both of my father and mother and all of family members for morale support, motivation and encouragement in completing this thesis for final year project and in finishing my study in UMP with successful.

Most important thanks here go to my husband, Ahmad Asnawi bin Alias. I don't know what my life would be without you. You are like the sunshine, always giving me the feeling of warmth, hope and peace. It is so wonderful to have you beside me, in the past, present, and future. Thanks for all your support.

I also would like to convey my full appreciation and thank you to my supervisor, Ass. Prof. Dr. MD. Maksudur Rahman Khan for his guidance, supervising and supporting me to complete my final year project for these two semesters. He has been very helpful and always advices me whenever there are problem in complete this project. I really appreciate every advice and without his support and critics, I am not being able to finish this thesis as presented here.

Dr Cheng Chin Kui, thank you for having your door open to any of my questions and problems, and also your time on checking my slide for presentation. My special thanks to friends that gives support and always company me in making and complete this project.

ABSTRACT

The aim of the present work is to synthesize and characterize P-type, N-type and P-N type photocatalysts for wastewater treatment, to compare photocatalytic activity of different catalysts for dye degradation and to study the effect of visible light irradiation of difference parameter of photocatalytic reaction. Multicomponent P-type and P-N type photocatalyst were synthesized and characterized by XRD, SEM and BET. The visible light is used to study the catalyst activity for the composition of dye using photocatalyst. However, the photocatalytic activity under visible light is low. In order to increase its activity, multi-component photocatalyst is used. P-N-type semiconductor is used as the photocatalysts as it improve the photocatalytic activity using couple catalyst by accelerating the separation of electron-hole pair as well as to efficiently extend the region of visible light utilization. This research will demonstrated the feasibilities of the photocatalytic degradation of Methylene Blue for treating wastewaters where it is depends by varying the initial concentrations of Methylene Blue, addition amounts of P-type photocatalyst and the light irradiation. As a result, the photocatalytic activity followed the series of $CaFe_2O_4$-V_2O_5 >> $CaFe_2O_4$-WO_3 > $CaFe_2O_4$. Based on the findings of this study, some recommendation can be made which are calcinations of the catalyst with different temperature, effect of visible light power intensity and effect of different dopants and their characterization by XRD and XPS.

ABSTRAK

Matlamat projek ini adalah untuk mensintesis dan mengenalpasti pemangkin cahaya jenis P, jenis N dan jenis P-N untuk merawat sisa air, bagi membandingkan aktiviti pemangkin cahaya bagi setiap jenis pemangkin untuk degradasi pewarna dan bagi mengkaji kesan cahaya nampak ke atas perbezaan parameter untuk reaksi kepada pemangkin cahaya. Pemangkin jenis P dan pemangkin multi-komponen jenis P-N telah disintesis dan dikenalpasti oleh XRD, SEM dan BET. Cahaya nampak digunakan untuk mengkaji aktiviti pemangkin bagi komposisi pewarna menggunakan pemangkin cahaya. Walau bagaimanapun, aktiviti pemangkin di bawah cahaya nampak adalah rendah. Bagi menaikkan aktiviti cahaya nampak, pemangkin multi-komponen telah digunakan. Semi-konduktor jenis P-N digunakan sebagai pemangkin kerana ia meningkatkan aktiviti pemangkin cahaya dengan mempercepatkan pembahagian lubang elektron dan cekap memanjangkan rantau cahaya nampak. Kajian ini akan menunjukkan kesesuaian metilena biru bagi merawat sisa air, di mana ia bergantung kepada kepekatan awal metilena biru, berat pemangkin cahaya yang digunakan dan penyinaran cahaya nampak. Sebagai kesimpulannya, aktiviti pemangkon cahaya adalah mengikut siri $CaFe_2O_4$-V_2O_5 >> $CaFe_2O_4$-WO_3 > $CaFe_2O_4$. Berdasarkan kajian yang dijalankan, beberapa cadangan boleh dibuat dengan membakar pemangkin cahaya pada suhu yang berbeza, mengenalpasti kesan perubahan ke atas kuasa keamatan cahaya nampak dan mengenalpasti kesan ke atas jenis dopan yang berbeza dan ciri-cirinya dengan menggunakan XRD dan XPS.

TABLE OF CONTENT

	Page
SUPERVISOR'S DECLARATION	i
STUDENT DECLARATION	ii
SPECIAL DEDICATION	iii
ACKNOWLEDGEMENTS	iv
ABSTRACT	v
ABSTRAK	vi
TABLE OF CONTENT	vii
LIST OF TABLES	x
LIST OF FIGURES	xi
LIST OF SYMBOLS	xiii
LIST OF ABBREVIATION	xiv
CHAPTER 1 INTRODUCTION	
1.1 Background of Study	1
1.2 Problem Statement	2
1.3 Research Objectives	3
1.4 Research Questions	3
1.5 Scope of Study	4
1.6 Significance of Study	4
1.7 Definition of key terms	5
1.8 Conclusion	5
CHAPTER 2 LITERATURE REVIEW	
2.1 Introduction	6
2.2 Multi-component Photocatalyst	6
2.2.1 P-type Semiconductor	7
2.2.2 N-type Semiconductor	8
2.2.3 P-N type Semiconductor	8

2.3 Reaction Mechanism 9

CHAPTER 3 METHODOLOGY

3.1 The Samples Materials 11
3.2 Apparatus and Istruments 12
3.3 Procedures 13
3.3.1 Preparation of P-type $CaFe_2O_4$ Catalyst 13
3.3.2 Preparation of P-N Junction Photocatalyst 14
3.4 Blank Test 14
3.5 Adsorption of Dye onto The Catalyst 14
3.6 Photoreactor and Procedure 15
3.7 Characterisation 16
3.7.1 X-Ray Diffraction (XRD) Analysis 16
3.7.2 Brunauer-Emmett-Teller (BET) Analysis 16
3.7.3 Scanning Electron Microscope (SEM) 16
3.7.4 UV-Vis Spectrophotometer Analysis 17
3.8 Photocatalytic Degradation Analysis 17

CHAPTER 4 RESULT AND DISCUSSION

4.1 Characterisation of P-Type $CaFe_2O_4$ Catalyst 18
4.1.1 XRD Analysis 18
4.1.2 BET Analysis 20
4.1.3 SEM Analysis 22
4.2 Characterisation of P-N Type Catalyst 23
4.2.1 XRD Analysis for $CaFe_2O_4$-WO_3 Catalyst 23
4.2.2 XRD Analysis for $CaFe_2O_4$-V_2O_5 Catalyst 24
4.2.3 BET Analysis for $CaFe_2O_4$-WO_3 Catalyst 25
4.2.4 BET Analysis for $CaFe_2O_4$- V_2O_5 Catalyst 26
4.2.5 Summary Report for BET Analysis 28
4.3 XRD Analysis of Compound Produce Catalysts 29
4.3.1 Calcium Oxide, CaO Compound 29

4.3.2 Iron Oxide, Fe_2O_5 Compound 30

4.3.3 Tungsten Oxide, WO_3 Compound 31

4.3.4 Vanadium Pentoxide, V_2O_5 Compound 32

4.4 Calibration Curve 33

4.5 Adsorption of Dye onto the Catalyst 34

4.6 Effect of Temperature on Photocatalyst Activity 36

4.6.1 Photocatalytic Activity at T= (45 ± 5) °C 36

4.6.2 Photocatalytic Activity at T= (30 ± 5) °C 37

4.7 Activity Evaluation of P-N Type Photocatalyst 39

4.7.1 $CaFe_2O_4$- V_2O_5 Photocatalyst 39

4.7.2 $CaFe_2O_4$-WO_3 Photocatalyst 40

4.8 Pseudo-First Order Kinetics 42

CHAPTER 5 CONCLUSION AND RECOMMENDATIONS

5.1 Introduction 45

5.2 Conclusion 45

5.3 Recommendations 46

REFERENCES 47

APENDICES 50

A1 Data of XRD $CaFe_2O_4$ Photocatalyst Analysis 50

A2 Data of XRD $CaFe_2O_4$-WO_3 Photocatalyst Analysis 53

A3 Data of XRD $CaFe_2O_4$-V_2O_5 Photocatalyst Analysis 56

A4 Data of XRD CaO Compound Analysis 59

A5 Data of Fe_2O_4 Compound Analysis 61

A6 Analysis of WO_3 Photocatalyst Analysis 63

A7 Data of XRD V_2O_5 Photocatalyst Analysis 67

B1 Data of BET $CaFe_2O_4$ Photocatalyst Analysis 70

B2 Data of BET $CaFe_2O_4$-WO_3 Photocatalyst Analysis 73

B3 Data of BET $CaFe_2O_4$-V_2O_5 Photocatalyst Analysis 76

C Data of SEM $CaFe_2O_4$ Photocatalyst Analysis 78

D Data of Adsorption Dye onto Catalyst 80

LIST OF TABLES

Table No.	Title	Page
3.1	Experimental materials	11
3.2	Experimental instrument	12
4.1	Surface area from BET analysis for $CaFe_2O_4$	20
4.2	Pore volume from BET analysis for $CaFe_2O_4$	21
4.3	Pore size from BET analysis for $CaFe_2O_4$	21
4.4	Surface area from BET analysis for $CaFe_2O_4$-WO_3	25
4.5	Pore volume from BET analysis for $CaFe_2O_4$-WO_3	25
4.6	Pore size from BET analysis for $CaFe_2O_4$-WO_3	26
4.7	Surface area from BET analysis for $CaFe_2O_4$- V_2O_5	27
4.8	Pore volume from BET analysis for $CaFe_2O_4$- V_2O_5	27
4.9	Pore size from BET analysis for $CaFe_2O_4$- V_2O_5	27
4.10	Summary Report for BET analysis	28
4.11	Calibration curve data	33
4.12	Result of adsorption of dye onto catalyst	34
4.13	The summary of rate constant for all photocatalyst	44

LIST OF FIGURE

Figure No.	Title	Page
2.1	Example of P-type semiconductor	7
2.2	Example of N-type semiconductor	8
2.3	P-N junction formation model and schematic diagram of electron hole separation process	10
3.1	The schematic diagram preparation of $CaFe_2O_4$ catalyst	13
3.2	The schematic diagram of photoreaction apparatus	15
4.1	XRD pattern for P-type $CaFe_2O_4$ catalyst	19
4.2	BET surface area plot for $CaFe_2O_4$	21
4.3	SEM analysis for P-type $CaFe_2O_4$ catalyst	22
4.4	XRD pattern for $CaFe_2O_4$-WO_3 catalyst	23
4.5	XRD pattern for $CaFe_2O_4$-V_2O_5 catalyst	24
4.6	BET surface area plot for $CaFe_2O_4$-WO_3	26
4.7	BET surface area plot for $CaFe_2O_4$- V_2O_5	28
4.8	XRD analysis for CaO compound	29
4.9	XRD analysis for Fe_2O_5 compound	30
4.10	XRD analysis for WO_3 Compound	31
4.11	XRD analysis for V_2O_5 compound	32
4.12	Calibration curve for Methylene Blue degeneration	33
4.13	Equilibrium study of methylene blue adsorption	36
4.14	Photocatalytic Reaction of $CaFe_2O_4$ Photocatalyst at T= (45 ± 5) °C	37
4.15	Photocatalytic Reaction of $CaFe_2O_4$ Photocatalyst at T= (30 ± 5) °C	38
4.16	Percentage removal of $CaFe_2O_4$ Photocatalyst at T= (30 ± 5) °C	38

4.17	Photocatalytic reaction of $CaFe_2O_4$-V_2O_5 photocatalyst at T= (30 ± 5) °C	40
4.18	Percentage removal of $CaFe_2O_4$-V_2O_5 photocatalyst at T=(30 ± 5)°C	40
4.19	Photocatalytic reaction of $CaFe_2O_4$-WO_3 photocatalyst at T= (30 ± 5) °C	41
4.20	Percentage removal of $CaFe_2O_4$-WO_3 photocatalyst at T= (30 ± 5) °C	41
4.21	Graph of ln(Co/C) versus time using $CaFe_2O_4$ photocatalyst	42
4.22	Graph of ln(Co/C) versus time curve using $CaFe_2O_4$-WO_3 Photocatalyst	43
4.23	Graph of ln(Co/C) versus time curve using $CaFe_2O_4$-V_2O_5 Photocatalyst	43

LIST OF SYMBOLS

η	Photocatalytic efficiency
C_0	Concentration of reactant before illumination
C_t	Concentration of reactant after illumination time t
B	Crystallite size
K	Scherrer constant
λ	Wavelength
L	Line broadening at half maximum intensity (FWHM)
Θ	Peak position
q	Kinetic rate constant
q_α	Maximum adsorption capacity
K	Adsorption equilibrium constant
C	Volume of methylene blue
w	Weight of photocatalyst
k	Rate constant
t	Illumination time

LIST OF ABBREVIATIONS

CdS	Cadmium Sulfate
CdSe	Cadmium Selenide
UV	Ultra violet
XRD	X-Ray diffraction
BET	Brunauer-Emmett-Teller
SEM	Scanning Electron Microscopy
B	Boron
Si	Silicon
Sb	Antimony
$CaFe_2O_4$	Calcium Iron Oxide
$Ca(NO_3)_2{\cdot}4H_2O$	Calcium Nitrate
$Fe(NO_3)_3{\cdot}9H_2O$	Iron Nitrate
NH_3	Ammonia
WO_3	Tungsten Oxide
V_2O_5	Vanadium Pentoxide
$C_{16}H_{18}N_3SCl$	Methylene Blue

CHAPTER 1

INTRODUCTION

1.1 BACKGROUND OF STUDY

Photocatalytic degradation of organic pollutants is one of the promising processes for environmental purification. The photocatalysis was revealed more than fifty years ago. Its use appeared in Japan in 1967, thanks to Professor Akira Fujishima. Researches and development continued and it was within the Japanese statecraft that the first realizations came out in 1990. The adventure of the photocatalysis can then expand rapidly in the European laboratories where it is set in numerous sectors and industrial applications: the building, the automobile or the household electrical appliances, the lighting and the sanitary (Carre, 2008).

Numerous studies have attempted to develop visible light driven photocatalysts in order to utilize solar energy and indoor light efficiently. There are two ways to exploit photocatalysts responsive to visible light irradiation (Tang *et al.*, 2004).

i. to generate intermediate energy levels in UV-active photocatalysts, such as TiO_2, by doping other elements to turn them into visible light photocatalysts
ii. to develop new materials with photocatalytic activity under visible light irradiation

Since few materials can provide both photo-oxidation power and photo-reduction power (which are necessary for complete decomposition of harmful

organics) and, at the same time, can absorb visible light efficiently, composite photocatalysts with two or more components were extensively explored, and improved photocatalytic performance was obtained from various composite photocatalysts. (Liu, 2009)

Previous studies of visible light photocatalysts are using unstable upon illumination of light for example CdS and CdSe and low photocatalytic activity. Recently, some UV active oxides functioned as visible light photocatalysts by substitutional doping of metals but these doped materials only show small absorption on visible light region (Kim, 2005).

Multi-component photocatalyst or couple catalyst is one of the new techniques that is used to improve the photocatalytic activities by accelerating the separation of electron-hole pairs and to efficiently extend the region of visible light utilization. Technology has been discovered that the photocatalytic activity of multi-component photocatalyst is higher than that of the single one itself. This is because some of single photocatalyst should satisfy the stringent requirements of both band gap energy and band position. When the single photocatalyst cannot meet these requirements, using the multi-component photocatalyst should be an alternative. (Kim, 2005).

It is known that $CaFe_2O_4$ is p-type semiconductor; meanwhile WO_3 and V_2O_5 are n-type semiconductor. Theoretically, when p-type $CaFe_2O_4$ and WO_3 or V_2O_5 form p–n junction, the photogenerated electrons and holes are separated efficiently, and the photocatalytic activity is enhanced. In this study, p-type $CaFe_2O_4$ powder was prepared by precipitation method. In the presence work, characterization methods were employed are XRD, BET and SEM.

1.2 PROBLEM STATEMENT

The water quality nowadays has becoming environmental major concerns. The fact that using energy to eliminate such environmental contamination will result unstable environmental impact, however, leads us to a dilemma not to use energy to

achieve our anti-pollution goal. Photocatalyst is a new material that can gently harmonize the contaminated environment to restore original conditions by using natural energy which is a part of the environment and low-cost energy supplied to our daily home life.

Mainly, photocatalytic is being done under ultra-violet (UV) light because it has more energy than visible light and mostly it generate suitable amount of energy for single photocatalyst to get excited. In this research, the visible light is use to treat the organic compound using photocatalytic. However, the photocatalytic activity under visible light is low. In order to increase its activity, multi-component photocatalyst is used.

1.3 RESEARCH OBJECTIVES

The objectives of this project are:

i. To synthesize and characterize P-type, N-type and P-N type photocatalysts for wastewater treatment
ii. To compare photocatalytic activity of different catalysts for dye degradation
iii. To study the effect of visible light irradiation of difference parameter of photocatalytic reaction.

1.4 RESEARCH QUESTIONS

i. What is the photocatalytic degradation efficiency of dye using P-N type photocatalyst?
iv. What is the comparison of the photocatalytic activity of different catalysts for dye degradation?
ii. What is the effect of visible light irradiation of difference parameter on photocatalytic reaction?

1.5 SCOPE OF STUDY

This research focuses on the synthesis P-type and P-N type photocatalyst for wastewater treatment under visible light irradiation by using precipitation method. The effect of visible light irradiation of difference parameter of photocatalytic reaction of this chosen system has also been studied and recorded. Methylene blue is used as the model substance.

The equipment that use in this experiment is Xenon Lamp and UV-Vis spectrophotometer.

1. In this research, the degradation process has been conducted at constant methylene blue concentration (50ppm). The catalyst amount is between 0.2-2.0 g.
2. The experiment carried out at two temperature condition which are T= (45 ± 5) °C and T= (30 ± 5) °C the irradiation process will be conducted from 0 min to 120 min.

Characterization of the catalysts was carried out using analytical instruments which include the X-Ray diffraction (XRD), Brunauer-Emmett-Teller (BET) and Scanning Electron Microscopy (SEM).

1.6 SIGNIFICANCE OF STUDY

With the significant increase in demand for water attention on reuse and recycling of wastewater has significantly increased. The method of photocatalytic degradation has many characteristics such as convenient safety, credibility and high efficiency. It helps to achieve standard pollution control and prevent environmental pollution**.** Thus, it is useful and advantageous to improve wastewater effluent. This technology can be commercialized for industrial application

1.7 DEFINITION KEY OF TERMS

i. Photocatalytic:

A process which a substance of photocatalyst introduces a chemical reaction under the action of the light, without undergoing any deterioration.

It is also a process by which free radicals are generated through the creation and subsequent separation of electron hole pairs formed in the presence of light, that are capable of breaking up complex organic molecules into smaller fragments

ii. Multi-component Photocatalyst:

A technique to improve the photocatalytic activity properties is by using couple catalyst where it used to accelerate the separation of electron-hole pair as well as to efficiently extend the region of visible light utilization.

iii. Visible Light :

Visible light is a range of electromagnetic radiation that can be detected by the human eye. The wavelengths associated with this range are 380 nm to 750 nm.

1.8 Conclusion

In conclusion, the method of photocatalytic degradation has many characteristics such as convenience, safety, credibility and high efficiency. So, it is hopeful that this method is extended and applied in the treatment of non-transparent or low-transparent wastewaters on the basic of more research work.

CHAPTER 2

LITERATURE REVIEW

2.1 INTRODUCTION

The Photocatalysis is a process in which a substance, the photocatalyst, introduces a chemical reaction under the action of the light, without undergoing any deterioration. It is also a process by which free radicals are generated through the creation and subsequent separation of electron hole pairs formed in the presence of light, that are capable of breaking up complex organic molecules into smaller fragments (Baruah, 2008). It used to degrade the material under the effect of the rays of light.

2.2 MULTI-COMPONENT PHOTOCATALYST

One technique to improve the photocatalytic activity properties is by using couple catalyst where it used to accelerate the separation of electron-hole pair as well as to efficiently extend the region of visible light utilization. This couple has been studied intensively by Chen Shifu *et al* and the result that the photocatalytic activity of couple catalyst is higher than that of the single one.

2.2.1 P-type Semiconductor

Generally, adding some percentage of foreign atoms in the regular crystal lattice will produce changes in its electrical properties for producing P-type and N-type semiconductor. This is also refers to the theory band of energy where extra levels have been added by the impurities for a certain energy to allow excitation of valance band electrons.

The P-type semiconductor can be defined as the addition of trivalent impurities to an intrinsic semiconductor that will create the deficiencies of valence electron, called “holes”. The **Figure 2.1** shows the example of P-type semiconductor where Boron is added into Silicon material and create extra hole of energy level.

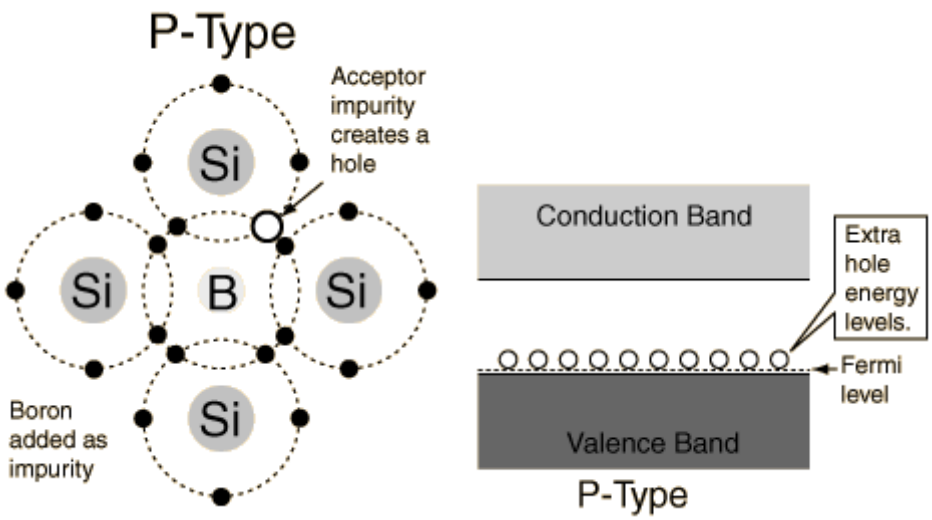

Figure 2.1: Example of P-type semiconductor

The addition of acceptor impurities contributes hole levels low in the semiconductor band gap so that electrons can be easily excited from the valence band into these levels, leaving mobile holes in the valence band. Electrons can be elevated from the valence band to the holes in the band gap with the energy provided by an applied voltage. Since electrons can be exchanged between the holes, the holes are

said to be mobile. The holes are said to be the "majority carriers" for current flow in a P-type semiconductor. (Nave, 2005)

2.2.2 N-type Semiconductor

N-type semiconductor is produce as the impurities of 5 valance electron (pentavalent impurities) is being contributed by extra electrons. The contribution of free electrons wills greatly increasing the conductivity of intrinsic semiconductor.

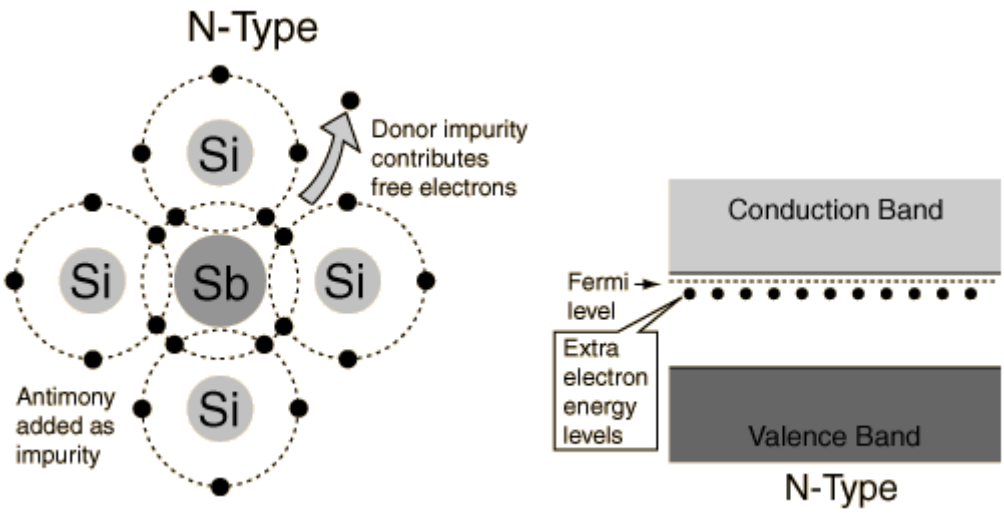

Figure 2.2: Example of N-type semiconductor

Referring to example of N-type semiconductor on **Figure 2.2,** the electrons can be elevated to the conduction band with the energy provided by an applied voltage and move through the material. The electrons are said to be the "majority carriers" for current flow in an N-type semiconductor (Nave, 2005).

2.2.1 P-N type Semiconductor

Photocatalyst should satisfy the stringent requirements of both gap energy and band positions. When the single component photocatalyst cannot meet these requirements, employment of multi-component photocatalyst should become an alternative. (Lee *et al.*, 2006)

There are 3 ways to combine the functions of different materials which are:

i. Simply mix an oxidation-type photocatalyst and reduction-type photocatalyst in a solution containing redox couple as electron shuttle
ii. Intercalate nano-particles of a photocatalyst into the layer of semiconductor
iii. Couple two semiconductors with different band position for efficient and longer charge separation

In photovoltaic cells that diode structure made of P-type and N-type semiconductor shows greatly enhanced activities compared to devices consisting of a single semiconductor (Khaselev, 1998). This formation of P-N type junction photocatalyst could lead to an efficient electron-hole separation that minimises the recombination of photo-excited electrons hole. (Jang *et al.*, 2007)

2.3 Reaction Mechanism

Photocatalytic activity mainly depends on whether the electron hole pairs can be separated effectively. Photocatalytic reaction is effective only when photo-excited electron holes can be captured or they will combine each other and give off heat on the surface of semiconductor. Refers to mechanism separation of electrons and holes, in order to increase photocatalytic activity two things must be considerate:

- To increase the separation efficiency of the photo-excited electron-hole pairs
- To increase the amount of photo-excited activity species

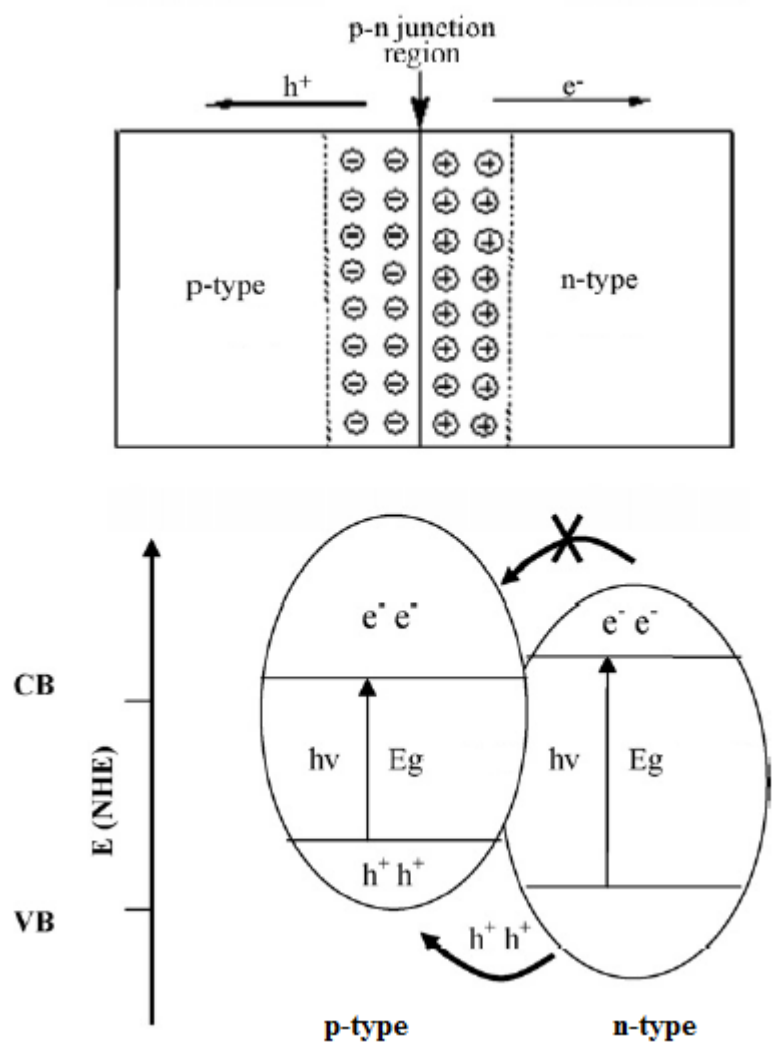

Figure 2.3: P-N junction formation model and schematic diagram of electron hole separation process

According to the position of band energy, the photo-excited holes can transfer from valence band of n-type to valance band of p-type but photo-excited electron cannot transfer from n-type to p-type because it will reduce the photocatalytic activity. The P-N junction formation model and schematic diagram of electron hole separation process is explained in **Figure 2.3**.

CHAPTER 3

RESEARCH METHODOLOGY

3.1 THE SAMPLES MATERIALS

To provide the P-N junction photocatalyst in this research, the P-type semiconductor that will be used is Calcium Iron Oxide, $CaFe_2O_4$. Meanwhile N-type catalysts which are Tungsten Oxide, WO_3 and Vanadium Pentoxide, V_2O_5 will be mixed with $CaFe_2O_4$ to produce couple catalyst.

The materials that will be used to prepare the P-N junction photocatalyst are as in the **Table 3.1** follow.

Table 3.1: Experimental materials

Name	Structure	Purity
Calcium Nitrate	$Ca(NO_3)_2 \cdot 4H_2O$	99%
Iron Nitrate	$Fe(NO_3)_3 \cdot 9H_2O$	99%
Ammonia	NH_3	30%
Tungsten Oxide	WO_3	99%
Vanadium Pentoxide	V_2O_5	99%
Methylene Blue	$C_{16}H_{18}N_3SCl$	99%

3.2 APPARATUS AND INSTRUMENTS

Table 3.2 shows experimental apparatus used in this experiment. A 75 W Xenon lamp was used to as the visible light to illuminate the solution.

Table 3.2: Experimental instruments

Apparatus	Model
Xenon Lamp 75w	HID
Stirring Hot Plate	Favorit
Shaking Water Bath	Lab. Companion
UV-Vis Spectrophotometer	Hitachi
Glass Furnace	Nabertherm
Oven	Memmert
Orbital Shaker	Certomat
Centrifuge Spin Rotor	Eppendorf

3.3 PROCEDURES

3.3.1 Preparation of P-type $CaFe_2O_4$ Catalyst

The preparation of P-type $CaFe_2O_4$ catalyst was adopted using sol–gel route to synthesize the $CaFe_2O_4$ nano-particles. A stoichiometric ratio of Calcium Nitrate, $Ca(NO_3)_2 \cdot 4H_2O$ and Iron Nitrate, $Fe(NO_3)_3 \cdot 9H_2O$ are mixed in 30% aqueous NH_3 solution, and the mixture was stirred at room temperature for 24 hours.

Then, heat the solution between ranges 70°C to 80°C and maintains the temperature at 80°C until the water evaporates, refer **Figure 3.1**. A kind of brown dry gel-like solution remained after evaporating the solvent. Finally, Calcium Iron Oxide powder was obtained by calcining the dry gel at 450°C for 2 hours and 1050°C for 10 hours using the furnace.

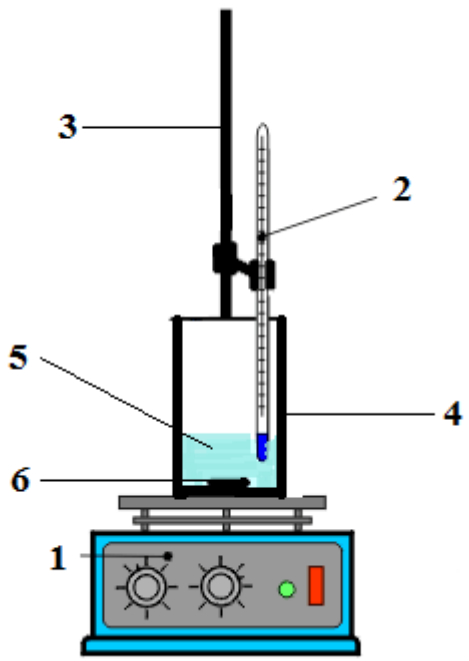

Figure 3.1: The schematic diagram preparation of $CaFe_2O_4$ catalyst: (1) magnetic agitator; (2) thermometer; (3) retort stand; (4) beaker; (5) solution; (6) magnetic stirrer

3.3.2 Preparation of P-N Junction Photocatalyst

For preparing the couple catalysts, the P-N junction of photocatalyst was produced by mixing $CaFe_2O_4$ and WO_3 powder with ratio of 1:10 in a quartz mortar with full hand force in the presence of small amount of deionised water. Then, the mixture is being dried in an oven at 60°C overnight. The procedures are repeated to produce $CaFe_2O_4$-V_2O_5 photocatalyst.

3.4 BLANK TEST

A given volume (100mL) of methylene blue solution of 50ppm was put into the beaker. The solution was irradiated by Xenon Lamp (75 W) for 7 hours without photocatalyst. Then, the UV/Vis spectrophotometer was used to analyse methylene blue concentration in the beaker.

3.5 ADSORPTION OF DYE ONTO THE CATALYST

The adsorption experiment was carried out with concentration of methylene blue solution of 50ppm, 75ppm, 100ppm, 150ppm and 200ppm. Each of the beakers contains 100mL of solution with 0.5 g of $CaFe_2O_4$ catalyst performed in a shaking water bath in the dark, without visible light irradiation. The solution was stirred at 100 rpm and temperature of 25°C for 8 hours. The samples volume of each is 5 mL was taken from the reaction suspension, centrifuged at 10 000 rpm for every 1 hour. Then the UV/Vis spectrophotometer was used to analyse methylene blue concentration left in the beaker.

3.6 PHOTOREACTOR AND PROCEDURE

Experiments were carried out in a photoreaction apparatus. **Figure 3.2** shows the schematic diagram of photoreaction apparatus. The apparatus consists of two parts. The first part is an annular quartz tube and the second part is an unsealed beaker volume 200 mL.

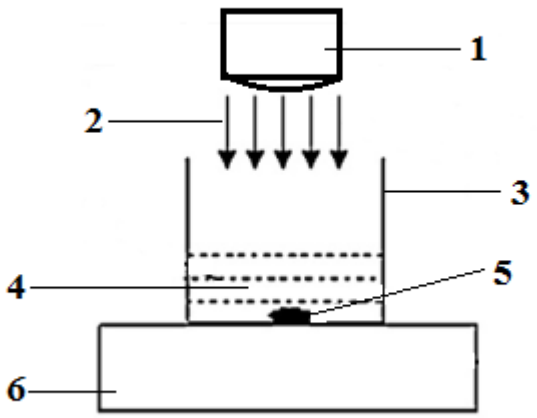

Figure 3.2: The schematic diagram of photoreaction apparatus: (1) xenon lamp; (2) light; (3) beaker; (4) reaction solution; (5) magnetic stirrer; (6) magnetic agitator

At the start of the experiment, the reaction solution of volume 100 mL containing reactants and photocatalyst was put in the unsealed beaker. A magnetic stirrer is used to stir the reaction solution. The distance between the light source and the surface of the reaction solution is set at 13 cm. In the experiment, the amount of photocatalyst used is varies, the initial concentration of Methylene Blue is 50 parts per million (ppm). The illumination time of each experiment is 120 minutes. In order to reach the adsorption–desorption equilibrium on the photocatalyst surface, the suspensions are magnetically stirred for 15 minutes prior to irradiation.

After illumination, the samples volume of each is 5 mL was taken from the reaction suspension, centrifuged at 10 000rpm for 10 min. The sample was then analyzed using UV-Vis Spectrophotometer. The blank test was also carried out by irradiating methylene blue solution without the photocatalyst for checking the photo-induced self-sensitised photodegradation.

3.7 CHARACTERISATION

The photocatalyst $CaFe_2O_4$, $CaFe_2O_4$- WO_3 and $CaFe_2O_4$-V_2O_5 was carried out to analyze physical and characteristics properties after preparation. X-ray diffraction (XRD) was used for analysis of catalyst crystalline, Brunauer-Emmett-Teller (BET) was used to measure the surface area of photocatalysts and UV-Vis Spectrophotometer was used to measure the photocatalytic degradation efficiency of methylene blue.

3.7.1 X-Ray Diffraction (XRD) Analysis

X-ray diffraction patterns were collected using X-ray diffractometer operated at accelerating voltage of 30 kV and emission current of 15 mA with graphite-monochromatized Cu Kα radiation and scanning speed 1°/min. The scanning step size 0.02° was over a range of 2θ = 20-80°.

3.7.2 Brunauer-Emmett-Teller (BET) Analysis

The BET surface area (S_{BET}), of the mixed oxide samples was measured by nitrogen sorption at -195.871°C using a BET adsorption unit. The catalyst samples were evacuated at 200°C for 1 h before measuring N2 adsorption isotherms.

3.7.3 Scanning Electron Microscope (SEM)

The microcrystalline structure and surface characteristics of the photocatalyst was investigated by using on the field emission scanning electron microscope (SEM).

3.7.4 UV-Vis Spectrophotometer Analysis

In order to investigate the optical and photochemical properties of the samples, UV–vis diffuse reflectance spectroscopy measurements were carried out using a Hitachi U-1800 Spectrophotometer. The analysis range was from 400 to 800 nm.

3.8 PHOTOCATALYTIC DEGRADATION ANALYSIS

The concentration of methylene blue (MB) in solution was determined by spectrophotometer. The photocatalytic degradation efficiency of methylene blue was calculated from the following expression:

$$\eta = \frac{C_0 - C_t}{C_0} \times 100$$

Where:

η = Photocatalytic efficiency

C_0 = Concentration of reactant before illumination

C_t = Concentration of reactant after illumination time *t*

CHAPTER 4

RESULT AND DISCUSSION

4.1 CHARACTERISATION OF P-TYPE $CaFe_2O_4$ CATALYST

The characterisation of P-type $CaFe_2O_4$ catalyst was carried out using X-Ray Diffraction (XRD) to determine the crystal phase composition and crystallite size of the photocatalyst, Brunauer-Emmett-Teller (BET) to measure the surface area of photocatalysts, Scanning Electron Microscope (SEM) to investigate the morphology of photocatalyst and UV-Vis Spectrophotometer was used to measure the photocatalytic degradation efficiency of methylene blue.

4.1.1 XRD Analysis

Figure 4.1 shows the XRD patterns of synthesized $CaFe_2O_4$ powder by calcining the sample at 450°C for 2 hours and 1050°C for 10 hours. It is obvious that the diffraction peaks at corresponding diffraction angles of anatase phase are 2θ= 33.69°, 35.56°, 49.79° and 61.42°.

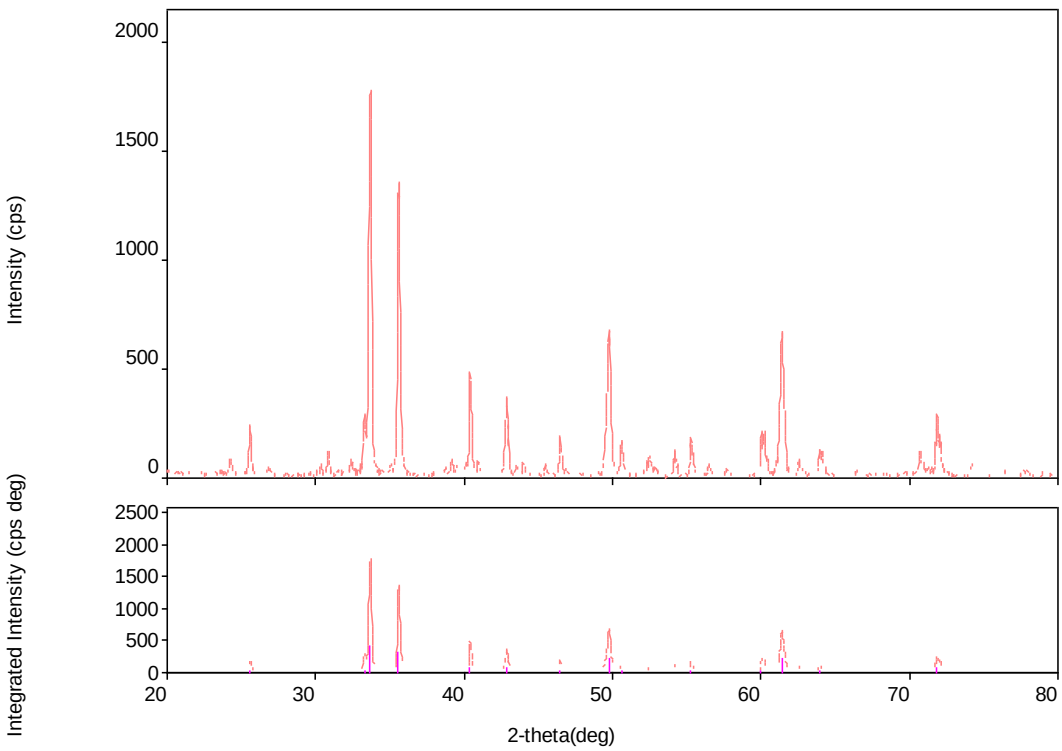

Figure 4.1: XRD pattern for P-type $CaFe_2O_4$ catalyst

The crystallite sizes of the P-type $CaFe_2O_4$ photocatalyst can be calculated from the X-ray peak broadening of the 33.69° diffraction peak using the Scherrer equation in **Eq 4.1** below.

$$B(2\theta) = \frac{K\lambda}{L\cos\theta} \qquad \textbf{Eq 4.1}$$

Where:

B = Crystallite size, nm

K = Scherrer constant, 0.94

λ = Wavelength, usually 1.54046 Å for Cu Kα

L = Line broadening at half maximum intensity (FWHM), °

Θ = Peak position, 2degree

From the analysis, the FWHM value of the sample at peak position 33.69° is 0.198°. The calculation of Scherrer equation shows that the crystallite size value is 8.97 nm. From the above results, it can be seen that, the sample has not only a small crystal size, but also a high crystallinity in this preparation condition.

4.1.2 BET Analysis

The porosity and specific surface area were determined by the modelling of N2 -adsorption data with the Brunauer–Emmett–Teller (BET) isotherm. The particle size distribution was determined by the fitting of an algorithm to patterns generated by the diffraction of a laser beam by suspended adsorbent particles. A surface area and porosity analyzer was used to perform textural analysis. The nitrogen used for this purpose was instrument-grade.

Textural characteristics of the tassel powder were determined by nitrogen adsorption–desorption at an analysis bath temperature of -195.871 °C with a warm free space of 26.6824 cm^3 and an equilibration interval of 5 seconds. The sample was automatically degassed. A sample mass of 0.1635 g was placed in a cold free space holder of 81.2935 cm^3. The adsorption–desorption isotherm, the BET surface area, the single-point adsorption total pore volume and the desorption average pore width were determined in **Table 4.1**, **Table 4.2** and **Table 4.3** and BET surface area was plot in **Figure 4.2.**

Table 4.1: Surface area from BET analysis for $CaFe_2O_4$

Analysis	Surface area
Single point surface area at P/Po = 0.300114832	2.4117 m^2/g
BET Surface Area	2.7560 m^2/g
Langmuir Surface Area	4.9457 m^2/g
t-Plot External Surface Area	4.1239 m^2/g
BJH Adsorption cumulative surface area of	3.528 m^2/g
BJH Desorption cumulative surface area of pores	6.1116 m^2/g

Table 4.2: Pore volume from BET analysis for $CaFe_2O_4$

Analysis	Surface area
Single point adsorption total pore volume of pores	0.0078 cm^3/g
Single point desorption total pore volume of pores	0.0073 cm^3/g
t-Plot micropore volume:	-0.001 cm^3/g
BJH Adsorption cumulative volume of pores	0.0084 cm^3/g
BJH Desorption cumulative volume of pores	0.0081 cm^3/g

Table 4.3: Pore size from BET analysis for $CaFe_2O_4$

Analysis	Surface area
Adsorption average pore width	112.8740 Å
Desorption average pore width	105.8673 Å
BJH Adsorption average pore diameter	96.117 Å
BJH Desorption average pore diameter	53.154 Å

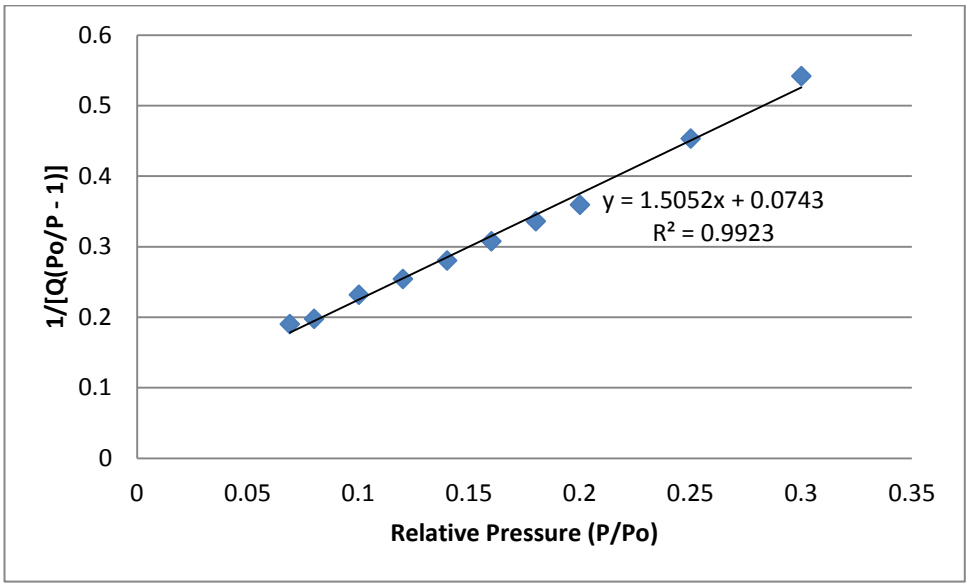

Figure 4.2: BET surface area plot for $CaFe_2O_4$

4.1.3 SEM Analysis

Scanning Electron Microscope (SEM) is used to analyse the microcrystalline structure and surface characteristics of the photocatalyst. **Figure 4.3** shows the microcrystalline structure of the $CaFe_2O_4$. It can be seen that the particle shape is spherical and the average diameter the photocatalyst is about 500-600nm.

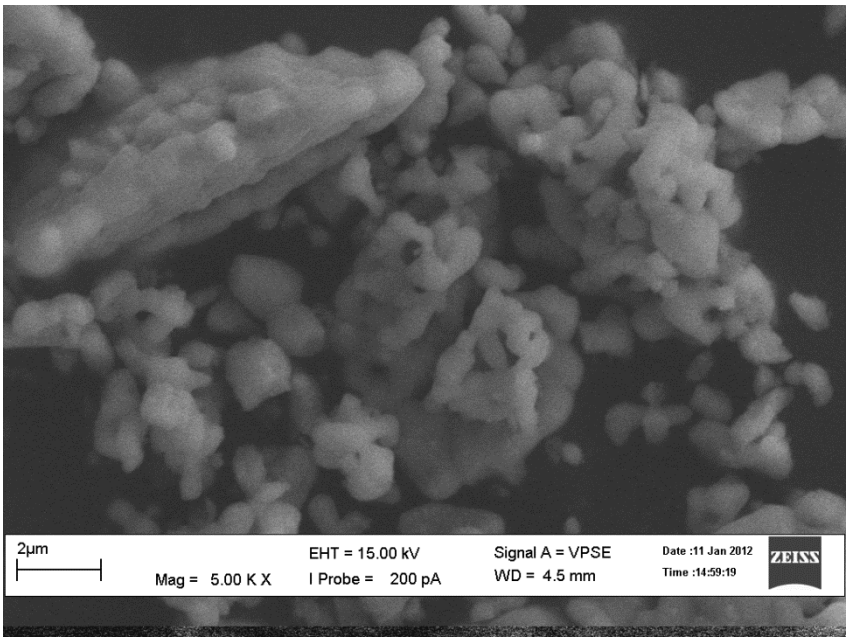

Figure 4.3: SEM analysis for P-type $CaFe_2O_4$ catalyst

4.2 CHARACTERISATION OF P-N TYPE CATALYST

4.2.1 XRD Analysis for $CaFe_2O_4$-WO_3 Catalyst

Figure 4.4 shows the XRD patterns of synthesized $CaFe_2O_4$-WO_3 catalyst powder by calcining the sample at 450°C for 2 hours and 1050°C for 10 hours. It is obvious that the diffraction peaks at corresponding diffraction angles of anatase phase are 2θ= 23.18°, 23.67°, 24.40°, 33.36°, 33.62° and 49.96°.

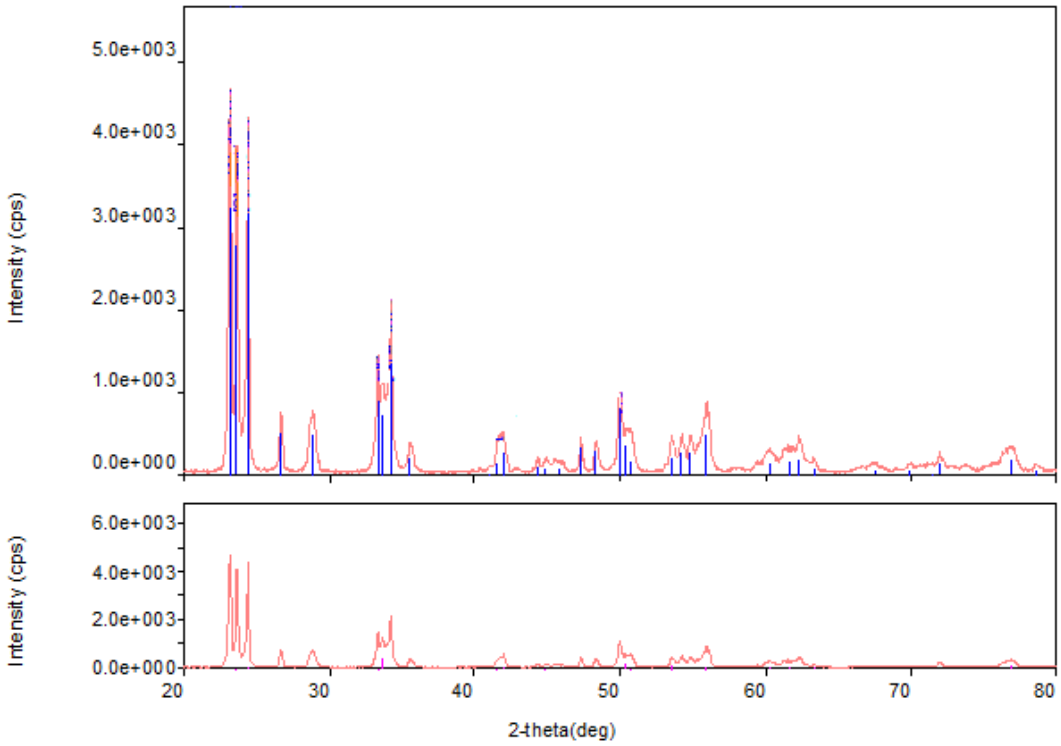

Figure 4.4: XRD pattern for $CaFe_2O_4$-WO_3 catalyst

The crystallite sizes of the P-N type $CaFe_2O_4$-WO_3 photocatalyst can be calculated from the X-ray peak broadening of the 23.18° diffraction peak using the Scherrer equation in **Eq. 4.1**. From the graph, the FWHM value of the sample at peak position 23.18° is 0.185°. The calculation of Scherrer equation shows that the crystallite size value is 8.69 nm.

4.2.2 XRD Analysis for $CaFe_2O_4$-V_2O_5 Catalyst

Figure 4.5 shows the XRD patterns of synthesized $CaFe_2O_4$-V_2O_5 catalyst powder by calcining the sample at 450°C for 2 hours and 1050°C for 10 hours. It is obvious that the diffraction peaks at corresponding diffraction angles of anatase phase are 2θ= 20.48°, 26.32° and 31.18°.

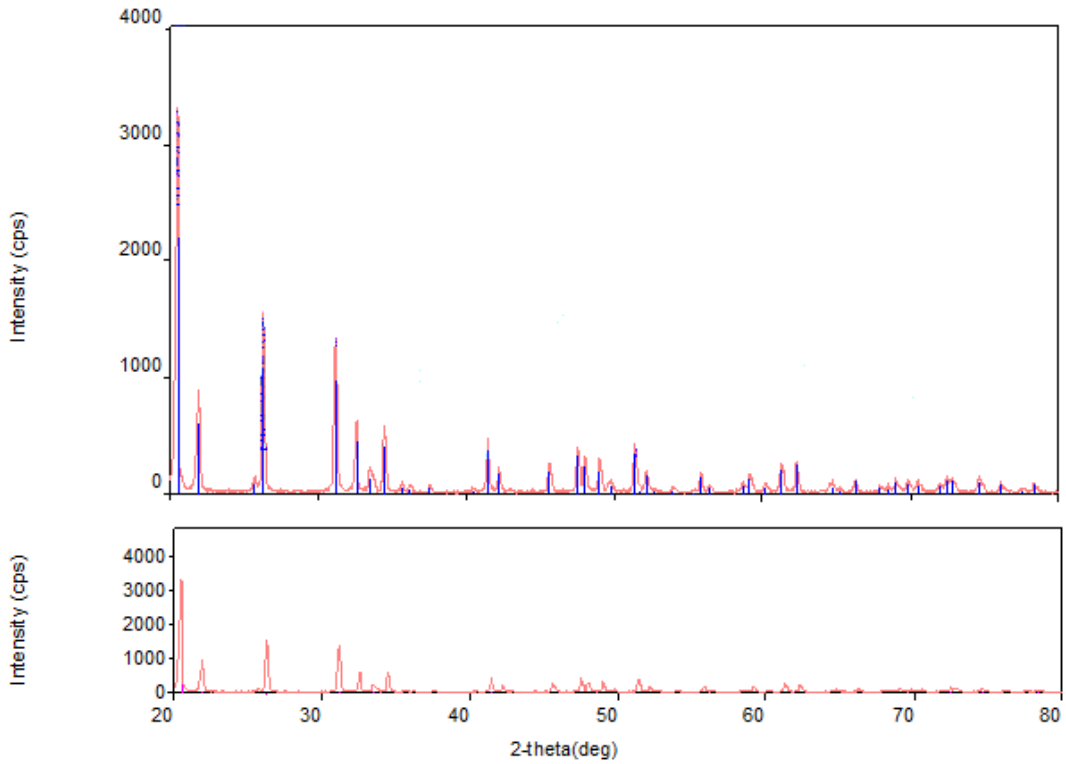

Figure 4.5: XRD pattern for $CaFe_2O_4$-V_2O_5 catalyst

The crystallite sizes of the P-N type $CaFe_2O_4$-V_2O_5 photocatalyst can be calculated from the X-ray peak broadening of the 20.48° diffraction peak using the Scherrer equation in **Eq. 4.1**. From the analysis, the FWHM value of the sample at peak position 20.48° is 0.214°. The calculation of Scherrer equation shows that the crystallite size value is 7.37 nm.

4.2.3 BET Analysis for $CaFe_2O_4$-WO_3 Catalyst

There are several conditions for BET used to analyse the $CaFe_2O_4$-WO_3 catalyst sample which are analysis bath temperature is set at -195.831 °C with a warm free space of 27.2397 cm^3 and an equilibration interval of 5 seconds. The sample was automatically degassed. A sample mass of 0.5759 g was placed in a cold free space holder of 82.2642 cm^3. The adsorption–desorption isotherm, the BET surface area, the single-point adsorption total pore volume and the desorption average pore width were determined in **Table 4.4, Table 4.5** and **Table 4.6** and BET surface area was plot in **Figure 4.6.**

Table 4.4: Surface area from BET analysis for $CaFe_2O_4$-WO_3

Analysis	Surface area
Single point surface area at P/Po = 0.300178917	2.2862 m^2/g
BET Surface Area	2.3159 m^2/g
Langmuir Surface Area	3.5976 m^2/g
t-Plot External Surface Area	1.8335 m^2/g
BJH Adsorption cumulative surface area of pores	1.520 m^2/g
BJH Desorption cumulative surface area of pores	2.0410 m^2/g

Table 4.5: Pore volume from BET analysis for $CaFe_2O_4$-WO_3

Analysis	Surface area
Single point adsorption total pore volume of pores	0.0003 cm^3/g
Single point desorption total pore volume of pores	0.0139 cm^3/g
t-Plot micropore volume:	0.0108 cm^3/g
BJH Adsorption cumulative volume of	0.0151 cm^3/g
BJH Desorption cumulative volume of pores	0.0152 cm^3/g

Table 4.6: Pore size from BET analysis for $CaFe_2O_4$-WO_3

Analysis	Surface area
Adsorption average pore width	186.7518 Å
Desorption average pore width	240.4644 Å
BJH Adsorption average pore diameter	397.099 Å
BJH Desorption average pore diameter	298.668 Å

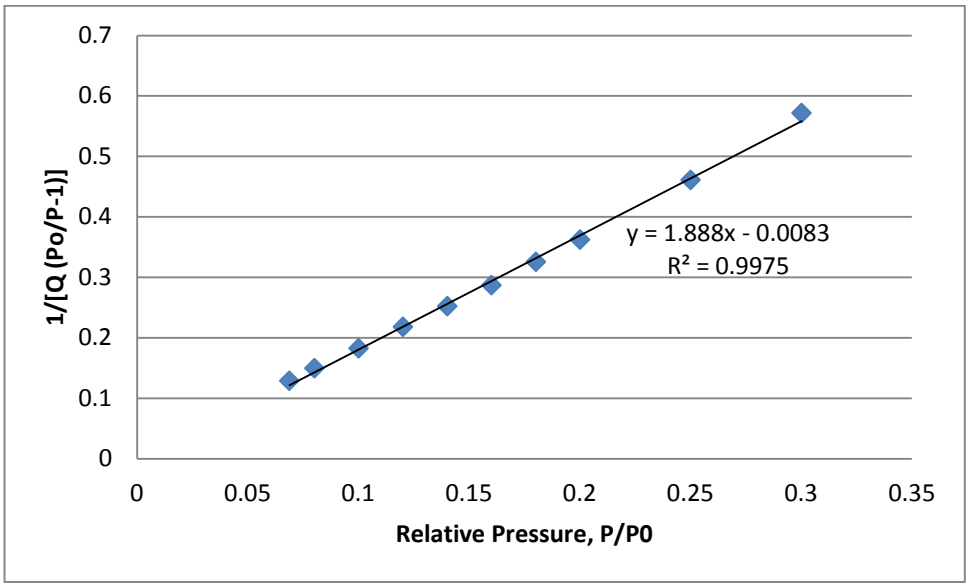

Figure 4.6: BET surface area plot for $CaFe_2O_4$-WO_3

4.2.4 BET Analysis for $CaFe_2O_4$- V_2O_5 Catalyst

There are several conditions for BET used to analyse the CaFe2O4- V2O5 catalyst sample which are analysis bath temperature is set at -195.857 °C with a warm free space of 27.1205 cm^3 and an equilibration interval of 5 seconds. The sample was automatically degassed. A sample mass of 0.2884 g was placed in a cold free space holder of 83.6602 cm^3. The adsorption–desorption isotherm, the BET surface area, the single-point adsorption total pore volume and the desorption average pore width were determined in **Table 4.7, Table 4.8** and **Table 4.9** and BET surface area was plot in **Figure 4.7.**

Table 4.7: Surface area from BET analysis for $CaFe_2O_4$- V_2O_5

Analysis	Surface area
Single point surface area at P/Po = 0.300178917	1.8928 m^2/g
BET Surface Area	1.8764 m^2/g
Langmuir Surface Area	2.6394 m^2/g
t-Plot External Surface Area	-3.4755 m^2/g
BJH Adsorption cumulative surface area of pores	0.455 m^2/g
BJH Desorption cumulative surface area of pores	0.6467 m^2/g

Table 4.8: Pore volume from BET analysis for $CaFe_2O_4$- V_2O_5

Analysis	Surface area
Single point adsorption total pore volume of pores	0.0051 cm^3/g
Single point desorption total pore volume of pores	0.0052 cm^3/g
t-Plot micropore volume:	0.0029 cm^3/g
BJH Adsorption cumulative volume of	0.0079 cm^3/g
BJH Desorption cumulative volume of pores	0.0079 cm^3/g

Table 4.9: Pore size from BET analysis for $CaFe_2O_4$- V_2O_5

Analysis	Surface area
Adsorption average pore width	109.5601 Å
Desorption average pore width	110.4056 Å
BJH Adsorption average pore diameter	696.580 Å
BJH Desorption average pore diameter	490.269 Å

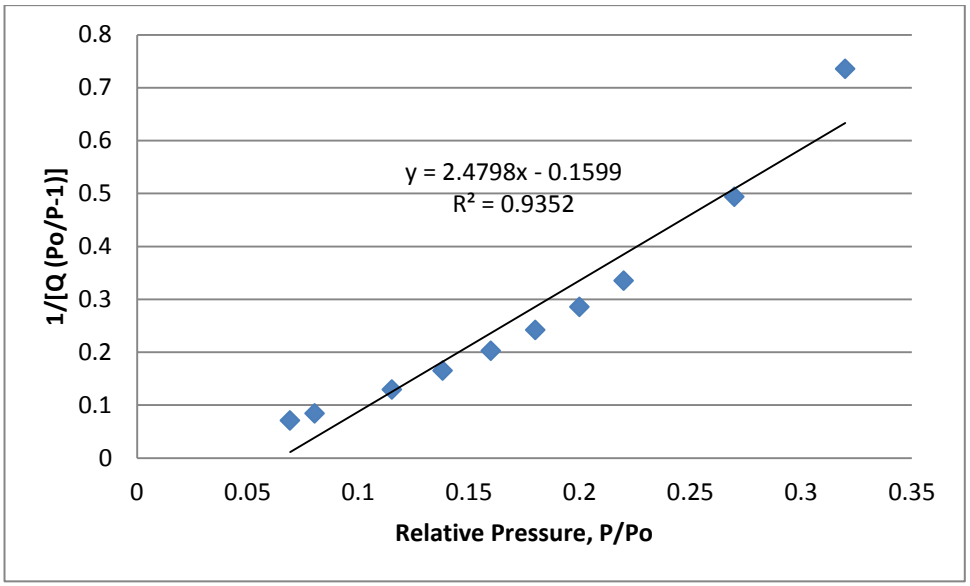

Figure 4.7: BET surface area plot for $CaFe_2O_4$- V_2O_5

4.2.5 Summary Report for BET Analysis

Table 4.10 shows the summary report for specific surface area, pore volume and pore size of main catalyst and couple catalyst experimentally measured by surface area analyzer, BET.

Table 4.10: Summary Report for BET analysis

	S_{BET} (m^2/g)	V_{pore} (cm^3/g)	D_{pore} (Å)
$CaFe_2O_4$	2.7560	0.0078	96.117
$CaFe_2O_4$-WO_3	2.3159	0.0003	397.099
$CaFe_2O_4$- V_2O_5	1.8764	0.0051	696.580

From the analysis above, we can say that the surface area and pore volume of $CaFe_2O_4$ catalyst is larger than $CaFe_2O_4$-WO_3 catalyst and $CaFe_2O_4$- V_2O_5 catalyst. Meanwhile the pore size for $CaFe_2O_4$ catalyst is smaller than $CaFe_2O_4$-WO_3 catalyst and $CaFe_2O_4$- V_2O_5 catalyst.

4.3 XRD ANALYSIS OF COMPOUND PRODUCE CATALYSTS

XRD analyses have been done to four types of compound that used to produce three types of catalyst. Calcium Nitrate, $Ca(NO_3)_2{\cdot}4H_2O$ and Iron Nitrate, $Fe(NO_3)_3{\cdot}9H_2O$ were used to produce the main catalyst which are Calcium Iron Oxide, $CaFe_2O_4$ photocatalyst. Meanwhile to produce the couple photocatalysts, Tungsten Oxide, WO_3 and Vanadium Pentoxide, V_2O_5 were mixed with $CaFe_2O_4$ catalyst to produce $CaFe_2O_4$-WO_3 catalyst and $CaFe_2O_4$- V_2O_5 catalyst.

These four types of compound need to be calcined before analyse by XRD using the same condition to produce photocatalyst which at 450°C for 2 hours and 1050°C for 10 hours. Calcium Nitrate, $Ca(NO_3)_2{\cdot}4H_2O$ has then become Calcium Oxide, CaO and Iron Nitrate, $Fe(NO_3)_3{\cdot}9H_2O$ has become Iron Oxide, FeO.

4.3.1 Calcium Oxide, CaO Compound

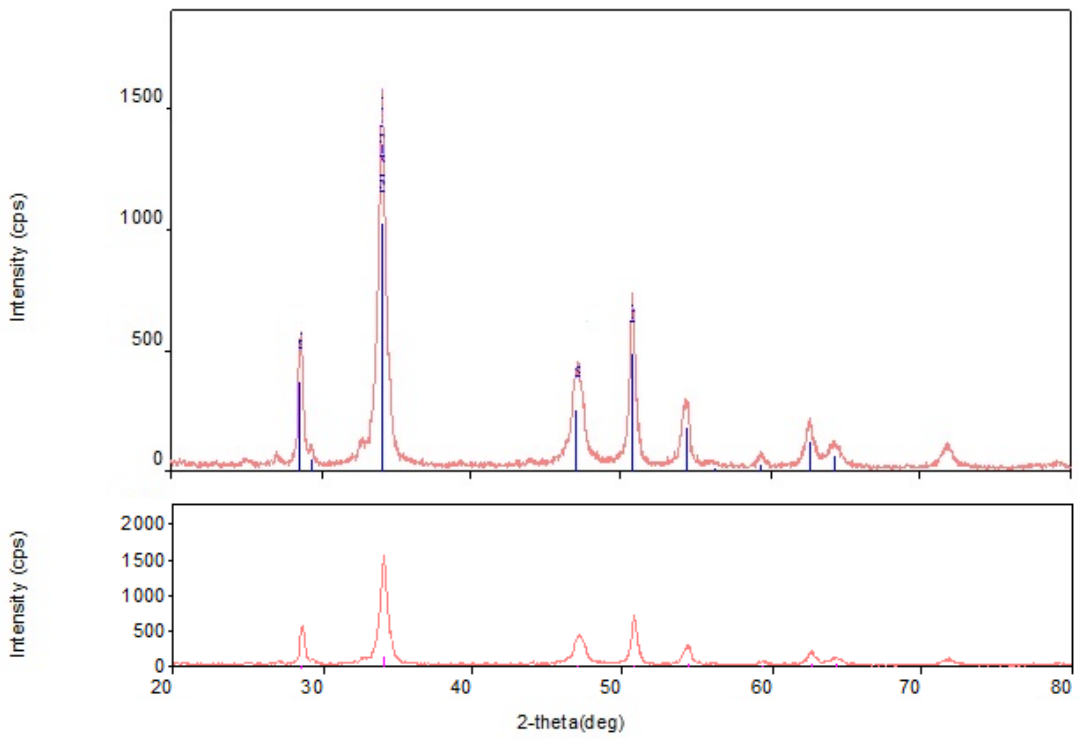

Figure 4.8: XRD analysis for CaO compound

Referring to **Figure 4.8**, the diffraction peaks at corresponding diffraction angles of anatase phase are 2θ= 28.65°, 34.03° and 50.69°. The crystallite sizes of CaO compound can be calculated from the X-ray peak broadening of the 34.03° diffraction peak using the Scherrer equation in **Eq. 4.1**. From the analysis, the FWHM value of the sample at peak position 34.03° is 0.585°. The calculation of Scherrer equation shows that the crystallite size value is 2.99 nm.

4.3.2 Iron Oxide, Fe_2O_5 Compound

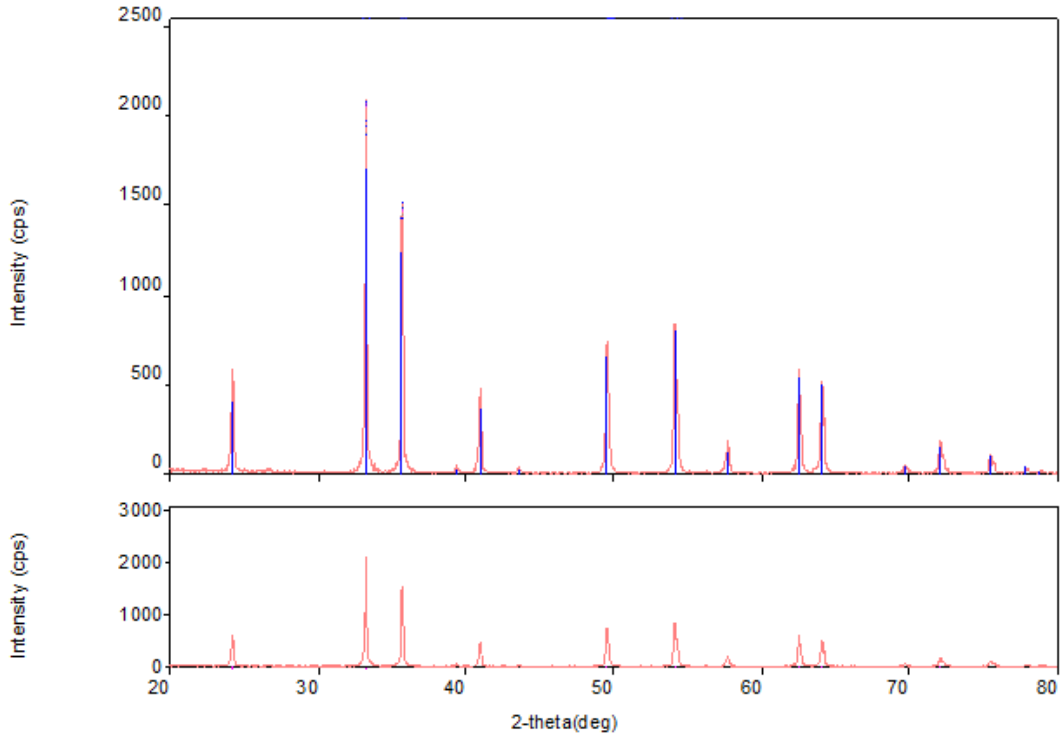

Figure 4.9: XRD analysis for Fe_2O_5 compound

Referring to **Figure 4.9**, the diffraction peaks at corresponding diffraction angles of anatase phase are 2θ= 33.23°, 35.69°, 49.53° and 54.15°. The crystallite sizes of Fe_2O_5 compound can be calculated from the X-ray peak broadening of the 33.23° diffraction peak using the Scherrer equation in **Eq. 4.1**. From the analysis, the FWHM value of the sample at peak position 33.23° is 0.138°. The calculation of Scherrer equation shows that the crystallite size value is 12.54 nm.

4.3.3 Tungsten Oxide, WO_3 Compound

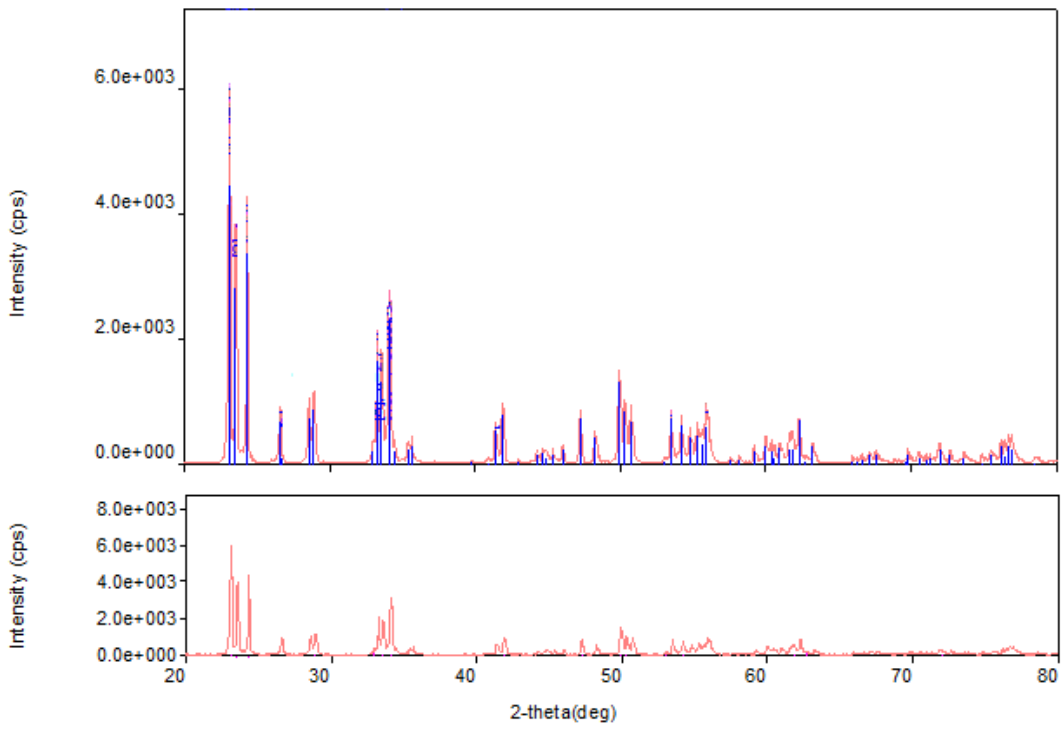

Figure 4.10: XRD analysis for WO_3 Compound

Referring to **Figure 4.10**, the diffraction peaks at corresponding diffraction angles of anatase phase are 2θ= 23.12°, 23.59° and 24.36°. The crystallite sizes of WO_3 compound can be calculated from the X-ray peak broadening of the 23.12° diffraction peak using the Scherrer equation in **Eq. 4.1**. From the analysis, the FWHM value of the sample at peak position 23.12° is 0.131°. The calculation of Scherrer equation shows that the crystallite size value is 12.02 nm.

4.3.4 Vanadium Pentoxide, V_2O_5 Compound

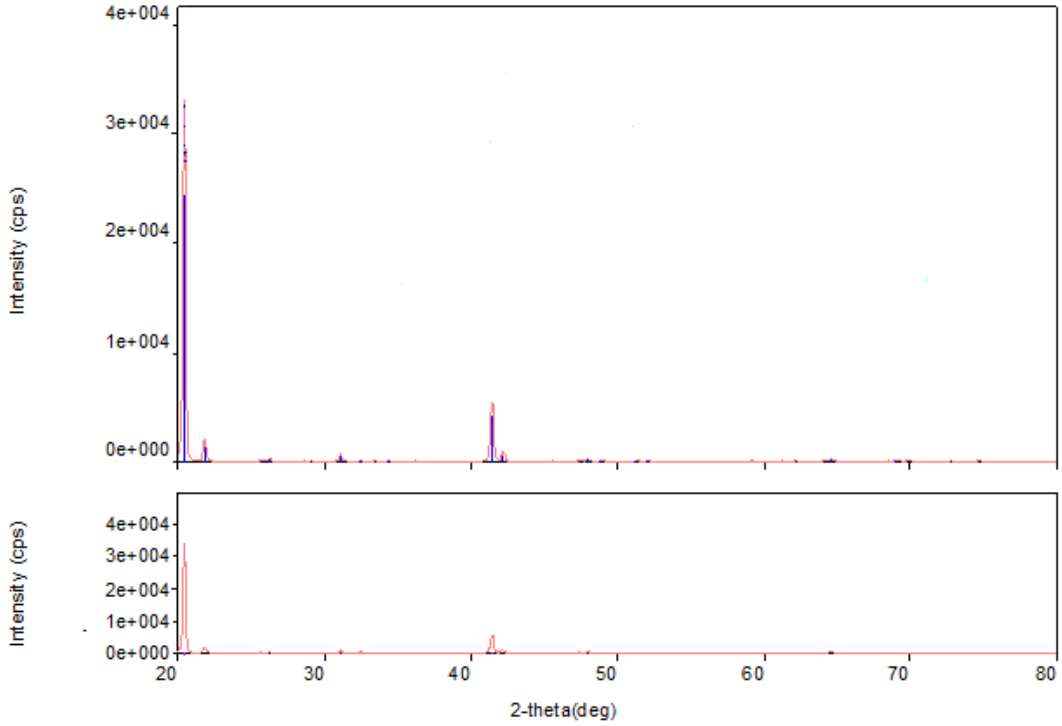

Figure 4.11: XRD analysis for V_2O_5 compound

Referring to **Figure 4.11**, the diffraction peaks at corresponding diffraction angles of anatase phase are 2θ= 20.43°, 21.85° and 42.17°. The crystallite sizes of V_2O_5 compound can be calculated from the X-ray peak broadening of the 20.43° diffraction peak using the Scherrer equation in **Eq. 4.1**. From the analysis, the FWHM value of the sample at peak position 20.43° is 0.173°. The calculation of Scherrer equation shows that the crystallite size value is 8.93 nm.

4.4 CALIBRATION CURVE

The concentration of methylene blue dye in the solution was determined using a calibration curve of methylene blue (concentration vs absorbance) prepared with known concentrations. The concentrations taken to prepare the calibration curve are 1ppm, 2ppm, 5ppm, 10ppm and 15ppm. The result and the graph of calibration curve are shown in **Table 4.11**.

Table 4.11: Calibration curve data

Concentration (ppm)	Absorbance (Abs)
1	0.048
2	0.401
5	1.096
10	2.009
15	2.658

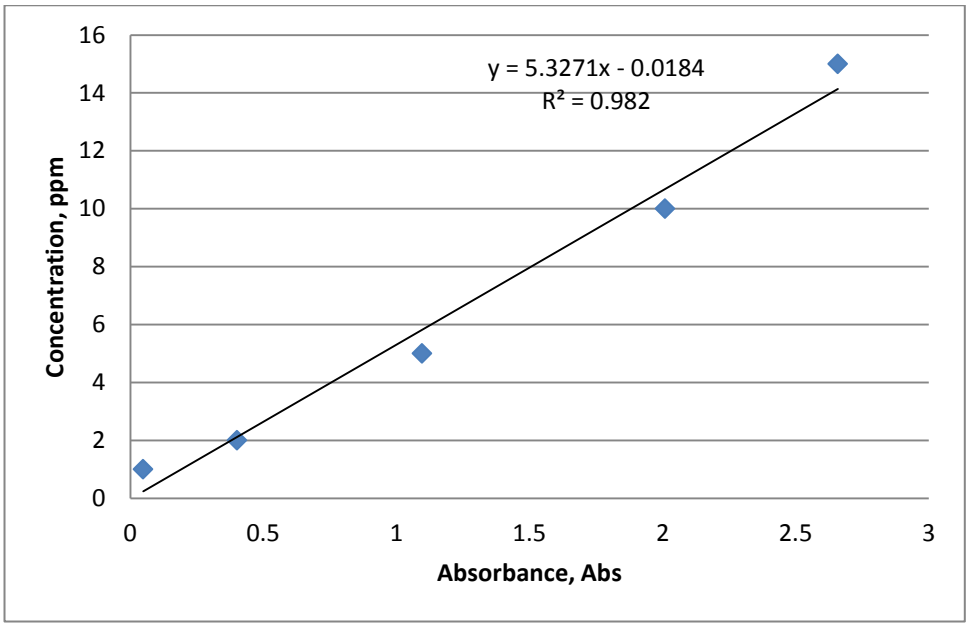

Figure 4.12: Calibration curve for Methylene Blue degeneration

Data given in **Table 4.11** is used to plot a graph of concentration versus absorbance in **Figure 4.12.** From this graph, the concentration of methylene blue dye in the solution can be determined using the linear equation of the graph which shown in **Eq 4.2** below.

$$y = 5.3271x - 0.0184 \qquad \textbf{Eq 4.2}$$

Where:

y = Concentration, ppm

x = Absorbance, abs

4.5 ADSORPTION OF DYE ONTO THE CATALYST

The adsorption experiment of methylene blue on the $CaFe_2O_4$ photocatalyst in the dark has been carried out at 25°C. It is the fast step to see whether the catalyst do adsorb the dye or not. The concentration was measured at maximum wavelength, λmax of 665nm. The result shows that adsorption amounts on the surface photocatalysts are low and there is little effect on the degradation efficiency. The concentration of methylene blue is determined for every one hour until it reaches the equilibrium concentration. The adsorption experiment result is shown in **Table 4.12**.

Table 4.12: Result of adsorption of dye onto catalyst

Initial Concentration, C_0 (ppm)	**Equilibrium Concentration, C_e (ppm)**
50	40.24
75	59.69
100	77.31
150	121.27
200	165

Using Langmuir equation in **Eq 4.3,** find the relation between the adsorption of catalyst to concentration of a medium above solid surface at fixed temperature using the equilibrium concentration obtained from adsorption experiment.

$$q = \frac{Kq_{\alpha}C}{1 + KC} \qquad \textbf{Eq 4.3}$$

$$\frac{1}{q} = \frac{1}{Kq_{\alpha}} \cdot \frac{1}{C} + \frac{1}{q_{\alpha}} \qquad \textbf{Eq 4.4}$$

$$q = (\frac{C_0 - C_e}{w})v \qquad \textbf{Eq 4.5}$$

Where:

q	=	Kinetic rate constant
q_{α}	=	Maximum adsorption capacity, mg/g
K	=	Adsorption equilibrium constant, L/mg
C	=	Equilibrium concentration, ppm
v	=	Volume of methylene blue, mL
w	=	Weight of photocatalyst, g

Arrange the Langmuir equation to be the linear equation just like in **Eq. 4.4.** The kinetic rate constant, q can be calculated using **Eq. 4.5**. Plot a graph of kinetic study of the methylene blue degradation (graph of $\frac{1}{C}$ vs $\frac{1}{q}$).

Referring to **Figure 4.13**, determine the adsorption equilibrium constant, K and the maximum kinetic rate constant, q_{α} using the equation of linear graph. From the calculation, the value obtained for adsorption equilibrium constant, K is 1.21×10^{-4} and the maximum adsorption capacity, q_{α} is 416.67.

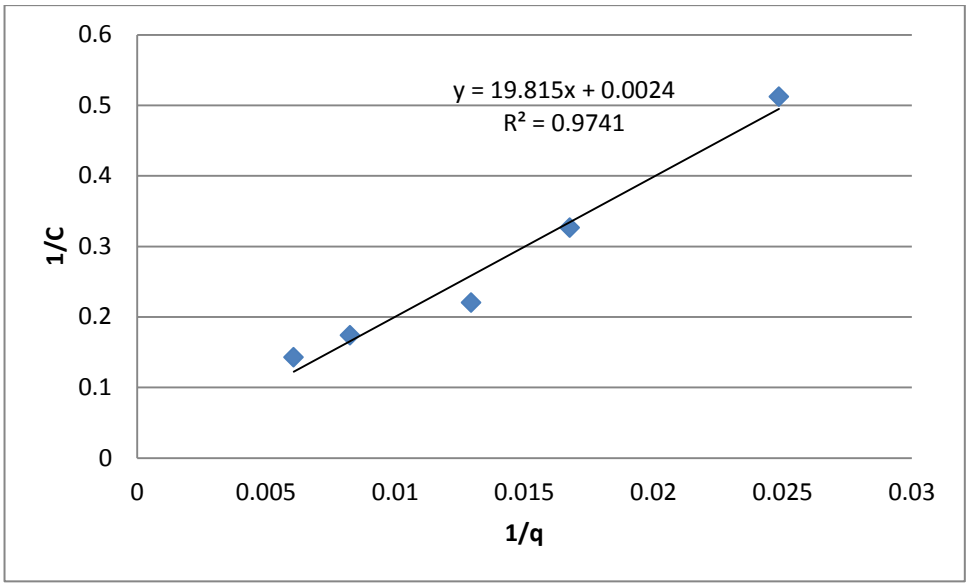

Figure 4.13: Equilibrium study of methylene blue adsorption

4.6 EFFECT OF TEMPERATURE ON PHOTOCATALYST ACTIVITY

In order to evaluate the photocatalytic activity of the $CaFe_2O_4$ photocatalyst, the experiment was conducted under visible light irradiation. The photocatalytic degradation reactions of methylene blue were carried out at different experimental condition which is relying on the effect of temperature. The first condition is by not controlling the temperature and the second condition is by controlling the temperature.

4.6.1 Photocatalytic Activity at T= (45 ± 5) °C

The first condition to evaluate the photocatalytic activity of the photocatalyst is without controlling the temperature. The illumination of the Xenon lamp is very high that cause the water begins to evaporate. There are three experiment have been conducted without controlling the temperature which are the blank test, photocatalytic reaction of 0.2 g $CaFe_2O_4$ photocatalyst and photocatalytic reaction of 0.6 g $CaFe_2O_4$ photocatalyst shown in **Figure 4.14**..

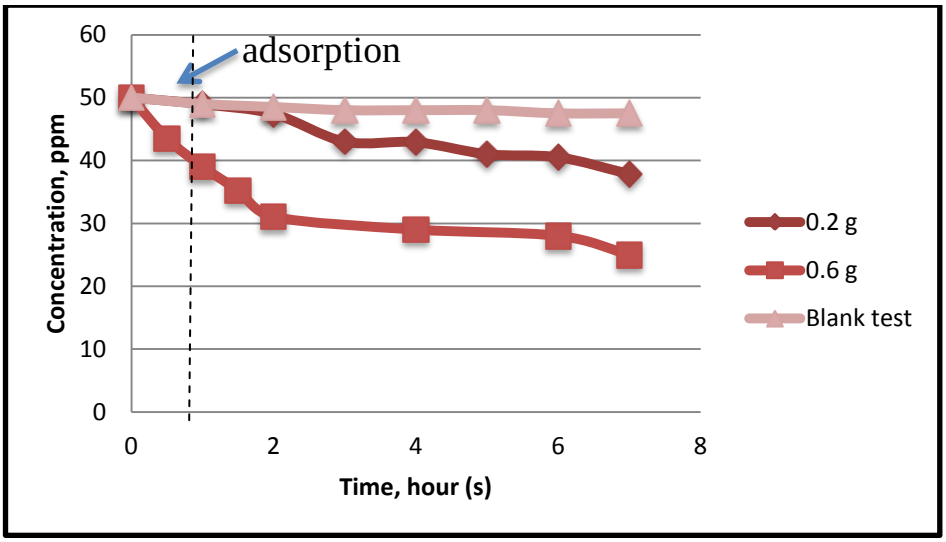

Figure 4.14: Photocatalytic Reaction of $CaFe_2O_4$ Photocatalyst at T= (45 ± 5) °C

The two results of photocatalytic reaction which are using 0.2 g of $CaFe_2O_4$ Photocatalyst and 0.6 g of $CaFe_2O_4$ photocatalyst shows that the low photocatalytic activity for both experiment. Where the photocatalytic activity increases as the amount of $CaFe_2O_4$ photocatalyst is increase.

Another reason is that the water starts to evaporate as the temperature increase. This results the concentration become high with small amount of water left in the beaker and making low in photocatalytic activity obtained for methylene blue.

4.6.2 Photocatalytic Activity at T= (30 ± 5) °C

The photocatalytic activity with controlling temperature is the step where the temperature is need to be maintain at T= (45 ± 5) °C. So, that, the water will be not evaporates while conducting the experiment. There are three experiment have been conducted by controlling the temperature which are the blank test, photocatalytic reaction of 1.0 g $CaFe_2O_4$ photocatalyst and photocatalytic reaction of 2.0 g $CaFe_2O_4$ photocatalyst. **Figure 4.15** shows the photocatalytic reaction of $CaFe_2O_4$ photocatalyst at difference catalyst dose.

Figure 4.16 shows the percentage removal of $CaFe_2O_4$. The percentage removal of 1.0 g $CaFe_2O_4$ photocatalyst is 21.4%. Meanwhile the percentage

removal of 2.0 g $CaFe_2O_4$ photocatalyst is 28.8% percentage degradation efficiency for 2 hours which is higher than 1.0 g $CaFe_2O_4$ photocatalyst.

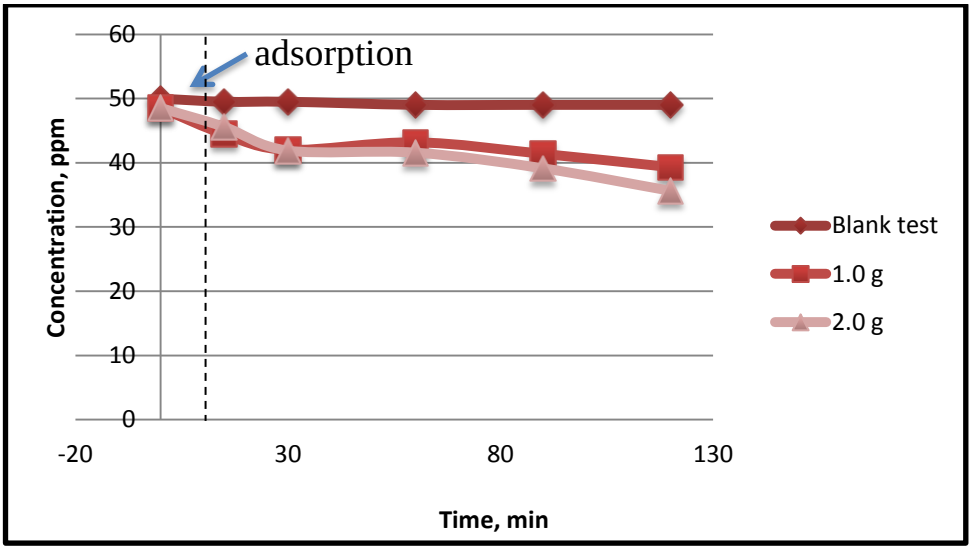

Figure 4.15: Photocatalytic Reaction of $CaFe_2O_4$ Photocatalyst at T= (30 ± 5) °C

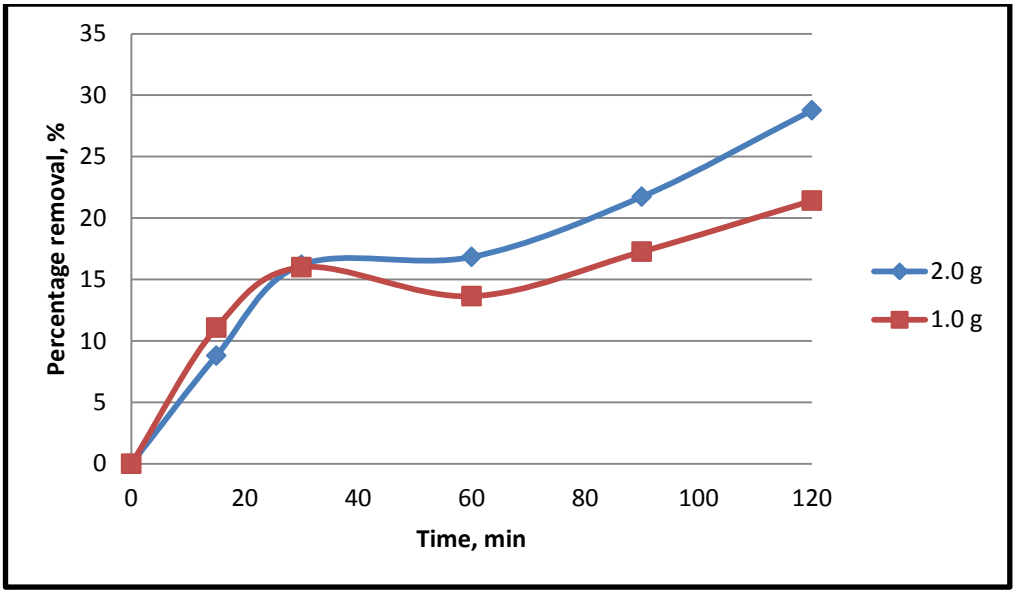

Figure 4.16: Percentage removal of $CaFe_2O_4$ Photocatalyst at T= (30 ± 5) °C

The percentage removal for $CaFe_2O_4$ Photocatalyst at T= (30 ± 5) °C is lower than percentage removal for $CaFe_2O_4$ Photocatalyst at T= (45 ± 5) °C. This is because the illumination of visible light no longer affects the solution.

4.7 ACTIVITY EVALUATION OF P-N TYPE PHOTOCATALYST

There are two types of P-N catalyst which are $CaFe_2O_4$-WO_3 catalyst and $CaFe_2O_4$-V_2O_5 catalyst. In order to evaluate the photocatalytic activity of the $CaFe_2O_4$ photocatalyst, the experiment was conducted under visible light irradiation. The photocatalytic degradation reactions of methylene blue were carried out by controlling the temperature.

4.7.1 $CaFe_2O_4$- V_2O_5 Photocatalyst

There are two experiment have been conducted by using $CaFe_2O_4$-V_2O_5 photocatalyst which are the photocatalytic reaction of 0.2 g $CaFe_2O_4$-V_2O_5 photocatalyst and photocatalytic reaction of 1.0 g $CaFe_2O_4$-V_2O_5 photocatalyst.

There are two experiment have been conducted by using $CaFe_2O_4$-V_2O_5 photocatalyst which are the photocatalytic reaction of 0.2 g $CaFe_2O_4$-V_2O_5 photocatalyst and photocatalytic reaction of 1.0 g $CaFe_2O_4$-V_2O_5 photocatalyst. **Figure 4.17** shows photocatalytic reaction of $CaFe_2O_4$-V_2O_5 photocatalyst.

The percentage of removal of 0.2 g $CaFe_2O_4$-V_2O_5 photocatalyst is found to be 96.3% for 2 hours. Meanwhile the percentage removal of 1.0 g $CaFe_2O_4$-V_2O_5 photocatalyst is 92% percentage degradation efficiency in 30 minutes. This shows that the activity for $CaFe_2O_4$-V_2O_5 photocatalyst way to much higher than the others. This because the pore size of $CaFe_2O_4$-V_2O_5 photocatalyst from BET characterisation is highest than other catalyst. The graph of percentage removal versus time is shown in **Figure 4.18.**

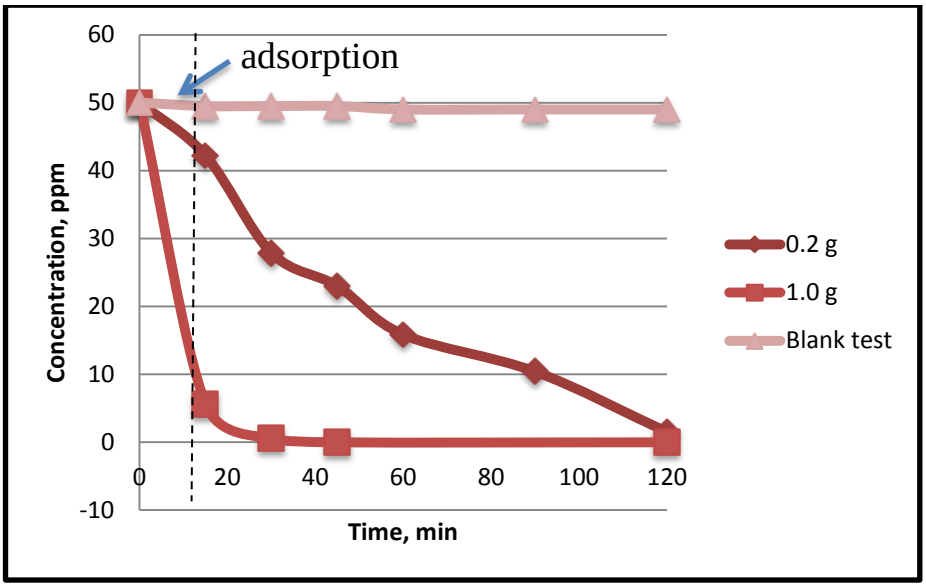

Figure 4.17: Photocatalytic reaction of $CaFe_2O_4$-V_2O_5 photocatalyst at T=(30 ± 5)°C

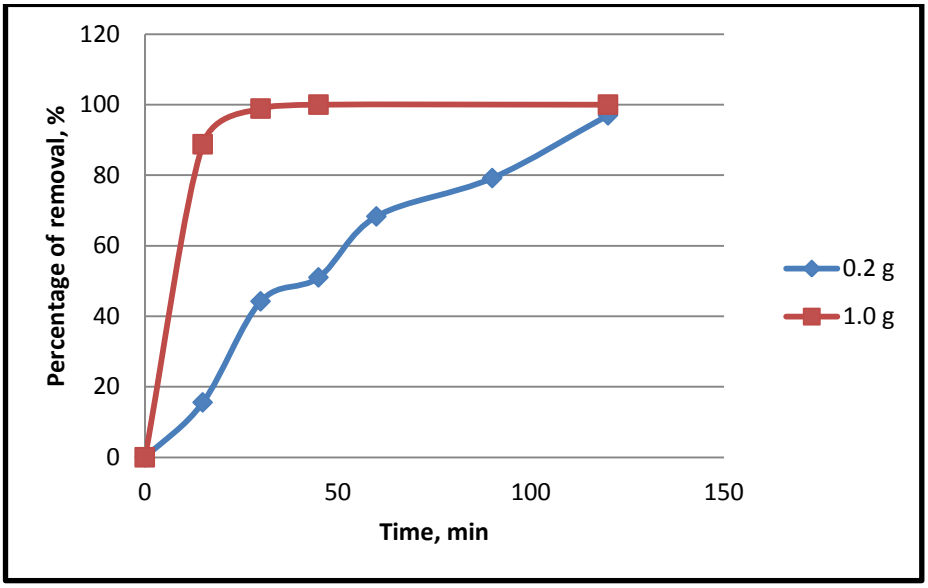

Figure 4.18: Percentage removal of $CaFe_2O_4$-V_2O_5 photocatalyst at T=(30 ± 5)°C

4.7.2 $CaFe_2O_4$-WO_3 Photocatalyst

There are two experiment have been conducted by using $CaFe_2O_4$-WO_3 photocatalyst which are the photocatalytic reaction of 0.2 g $CaFe_2O_4$-WO_3 photocatalyst and photocatalytic reaction of 1.0 g $CaFe_2O_4$-WO_3 photocatalyst.

Figure 4.19 shows photocatalytic reaction of $CaFe_2O_4$-WO_3 photocatalyst. The percentage removal of 0.2 g $CaFe_2O_4$-WO_3 photocatalyst if found to be 64% for 2 hours. Meanwhile the percentage removal of 1.0 g $CaFe_2O_4$-WO_3 photocatalyst is 89.8% percentage degradation efficiency for 2 hours. This because the pore size of $CaFe_2O_4$-WO_3 photocatalyst from BET characterisation is between the other catalysts. The graph of percentage removal versus time is shown in **Figure 4.20.**

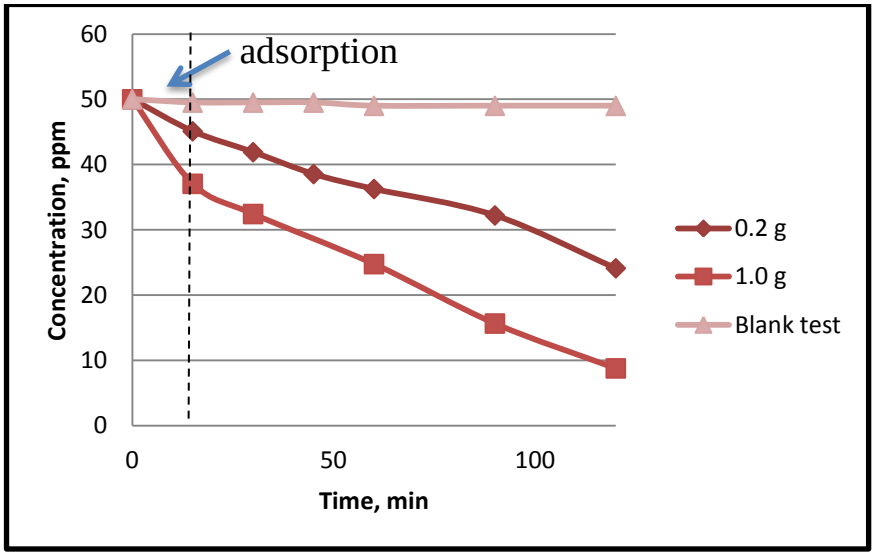

Figure 4.19: Photocatalytic reaction of $CaFe_2O_4$-WO_3 photocatalyst at T=(30 ± 5)°C

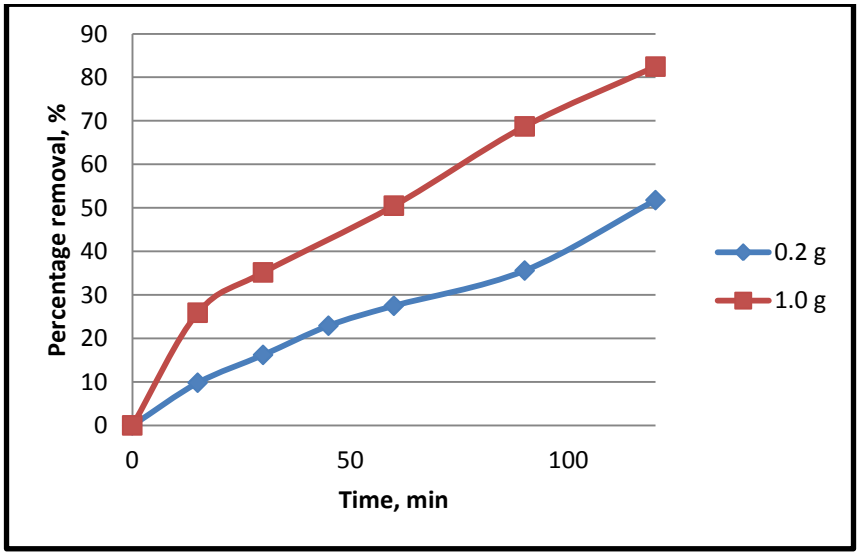

Figure 4.20: Percentage removal of $CaFe_2O_4$-WO_3 photocatalyst at T=(30 ± 5)°C

4.8 PSEUDO-FIRST ORDER KINETICS

Photodegradation processes of the organic compounds were adequately fitted by a pseudo-first-order kinetic treatment in the presence of IPCA catalyst studied in this work. Loss of the model pollutant was fitted to the following logarithmic expression:

$$\ln\left(\frac{C_0}{C}\right) = kt \qquad \textbf{Eq. 4.6}$$

Where C_0 and C represent the concentration of the substrate in solution at the time zero and time *t* of illumination, respectively, and *k* represents the apparent rate constant. This is an empirical rate law reflecting a complex of factors including competition between the primary substrate and intermediates. The graph plot of ln(Co/C) versus time for difference photocatalyst shown in **Figure 4.21**, **Figure 4.22** and **Figure 4.23**. The summary of rate constant for all photocatalyst is state in **Table 4.13**.

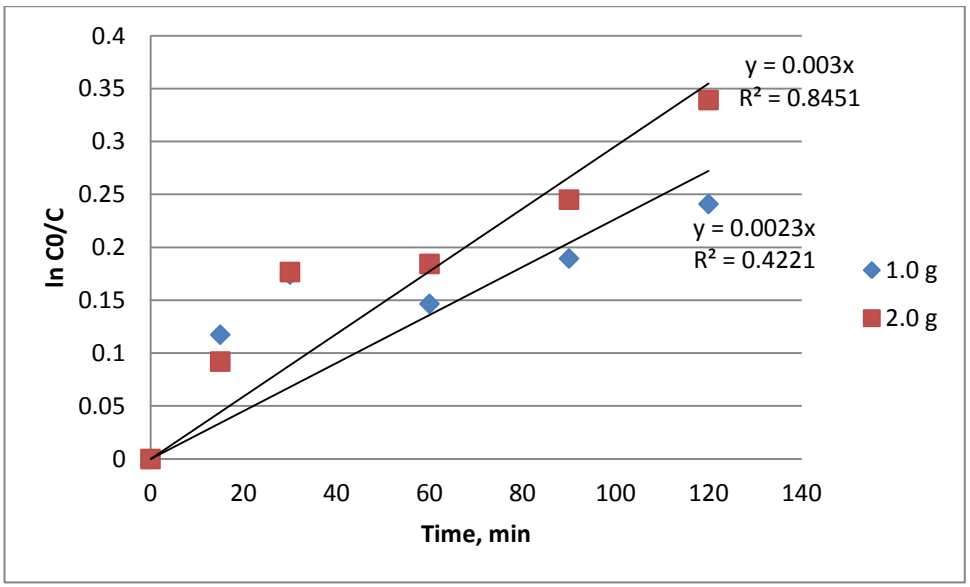

Figure 4.21: Graph of ln(Co/C) versus time using $CaFe_2O_4$ photocatalyst

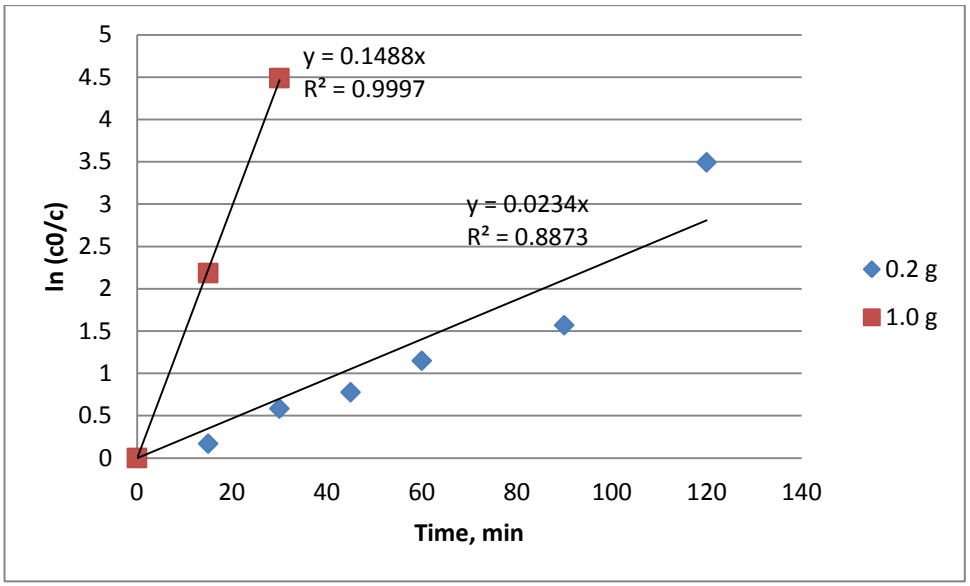

Figure 4.22: Graph of ln(Co/C) versus time curve using $CaFe_2O_4$-WO_3 photocatalyst

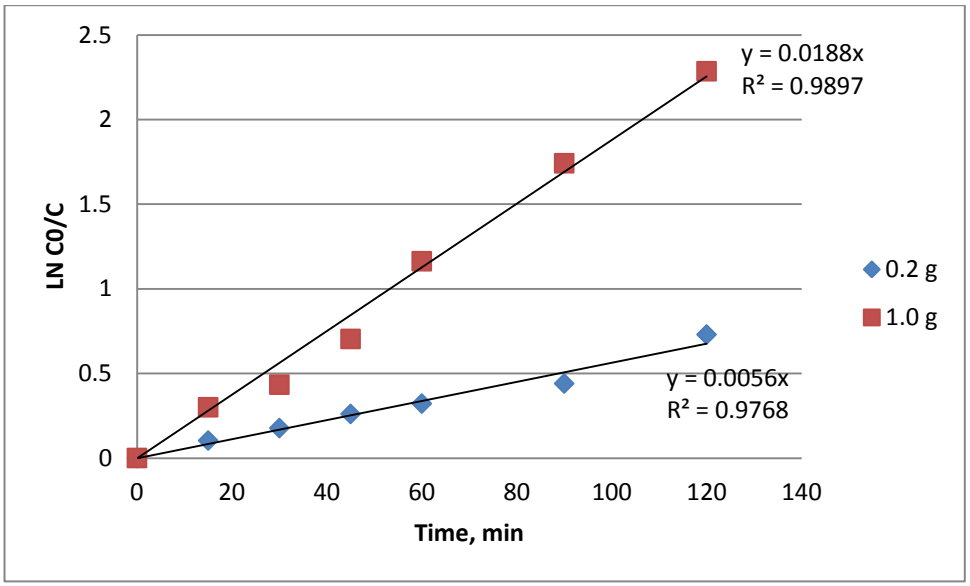

Figure 4.23: Graph of ln(Co/C) versus time curve using $CaFe_2O_4$-V_2O_5 photocatalyst

Table 4.13: The summary of rate constant for all photocatalyst

Photocatalyst	Dose (g)	Rate constant, k (min^{-1})
$CaFe_2O_4$	1.0	0.0023
	2.0	0.003
$CaFe_2O_4$-WO_3	0.2	0.0056
	1.0	0.0188
$CaFe_2O_4$-V_2O_5	0.2	0.0234
	1.0	0.1488

CHAPTER 5

CONCLUSION AND RECOMMENDATION

5.1 INTRODUCTION

This chapter is the summary of what this whole research is about. It concludes all the outcomes, observation of results and analysis, and discussion throughout the experiment. Recommendations may also be given on improving future work and studies.

5.2 CONCLUSION

Efficient visible light active $CaFe_2O_4$, $CaFe_2O_4$-WO_3 and $CaFe_2O_4$-V_2O_5 photocatalysts were prepared, and the photocatalytic performance was investigated. It is successfully achieving the objectives with the acceptable result outcome.

The synthesis of photocatalysts has been done using precipitation method and photocatalysts were characterized by SEM, XRD and BET. The result of BET shows that the surface area and pore volume of $CaFe_2O_4$ catalyst is larger than $CaFe_2O_4$-WO_3 catalyst and $CaFe_2O_4$- V_2O_5 catalyst. Meanwhile the pore size for $CaFe_2O_4$ catalyst is smaller than $CaFe_2O_4$-WO_3 catalyst and $CaFe_2O_4$- V_2O_5 catalyst.

Meanwhile, from adsorption of dye onto the $CaFe_2O_4$ photocatalyst by using the Langmuir isotherm shows that the value obtained for adsorption equilibrium constant, K is 1.21×10^{-4} and the maximum adsorption capacity, q_α is 416.67. The

result shows that adsorption amounts on the surface photocatalysts are low and there is little effect on the degradation efficiency.

The result obtain in the research shows that the photocatalytic activity followed the series of $CaFe_2O_4$-V_2O_5 >> $CaFe_2O_4$-WO_3 > $CaFe_2O_4$. The amount of catalyst doped is al so affecting the photocatalytic activity as well as the percentage of removal for the methylene blue. The higher amount of catalyst used, the higher photocatalytic activity for the photocatalyst.

5.3 RECOMMENDATIONS

Based on the findings of this study the following recommendation can be made. The suggestions are as follows:

i. Surface modification can be made by heating the catalyst with different temperature
ii. The photocatalytic activity can be largely improve by coating the particle surface of catalyst with Ag or ITO layer
iii. The photocatalytic activity enhancement is attributed to the efficient charge separation resulting from recombination of the photogenerated charge carriers at ohmic contact interface.
iv. The calcinations of the catalyst with different temperature,
v. Controlling the visible light power intensity
vi. Use different dopants and analyse their characterisation by XRD and XPS.

REFERENCES

M. Zhang, C.C. Chen, W.H. Ma, J.C. Zhao, Visible-light-induced aerobic oxidation of alcohols in a coupled photocatalytic system of dye-sensitized TiO2 and TEMPO, Angew. Chem. Int. Ed. 47 (2008)

Q. Wang, C.C. Chen, D. Zhao, W.H. Ma, J.C. Zhao, Change of adsorption modes of dyes on fluorinated TiO2 and its effect on photocatalytic degradation of dyes under visible irradiation, Langmuir 24 (2008)

Jae Sung Lee, Photocatalytic water splitting under visible light with particulate semiconductor catalysts, Department of Chemical Engineering, POSTECH (2006)

S. Chen, W. Zhao, W. Liu, H. Zhang, X. Yu, Y. Chen, Preparation, characterization and activity evaluation of p-n junction photocatalyst p-CaFe2O4/n-Ag3VO4 under visible light, Elsevier B. V. (2009)

H.G. Kim, H.B. Pramod, J.S. Lee, Photocatalytic nanodiodes for visible-light photocatalysis, Angew. Chem. Int. Ed. 44 (2005)

H. Carre, The photocatalysis: A technology of a depolluting by generating the living environment and improving it in sustainable development way, Federation Fraincaise de la Photocatalyse (2008)

S.F. Chen, S.J. Zhang, W. Liu, W. Zhao, Preparation and activity evaluation of p–n junction photocatalyst NiO/TiO2, J. Hazard. Mater. 115 (2008)

J. M. Joseph, H. Destaillats, H.M. Hung and M.R. Hoffmann, J. Phys. Chem. A (2000)

Y. Yonezawa, R. Hanawa, and H. Hada, Application of a membrane cell to the study of photo electrochemical processes at a TiO2 solution interface, *Journal of Imaging Science, vol. 29,* no. 5, pp. 171–174 (1985)

S.X. Liu, H. Liu, Fundamental and Application of Photocatalysis and Electrophotocatalysis, first ed., Chem Ind., Beijing (2005)

Z. Liu, Z. Zhou, M.Miyauchi, Efficient visible light active CaFe2O4/WO3 based composite Photocatalysts: Effect of interfacial modification (2009)

Y. Yonezawa, R. Hanawa, and H. Hada, Application of a membrane cell to the study of photo electrochemical processes at a TiO2 solution interface, *Journal of Imaging Science, vol. 29,* no. 5, pp. 171–174 (1985)

C. Shifu, Z. Wei, L. Wei, Z. Huaye and Y. Xiaoling, Preparation, characterization and activity evaluation of p-n junction photocatalyst p-CaFe2O4/n-ZnO under visible light (2009)

W.Y. Su, Y.F. Zhang, Z.H. Li, L. Wu, X.X. Wang, J.Q. Li, X.Z. Fu, Multivalency iodine doped TiO2: preparation, characterization, theoretical studies, and visible-light photocatalysis, Langmuir 24 (2008)

X.X. Hu, C. Hu, Preparation and visible-light photocatalytic activity of Ag3VO4 powders, J. Solid State Chem. 180 (2007)

D.Z. Li, Z.X. Chen, Y.L. Chen, W.J. Li, H.J. Huang, Y.H. He, X.Z. Fu, A new route for degradation of volatile organic compounds under visible light: Using the bifunctional photocatalyst Pt/TiO2-xNx inH2O2 atmosphere, Environ. Sci. Technol. 42 (2008)

C.C. Chen, Q. Wang, P.X. Lei, W.J. Song, W.H. Ma, J.C. Zhao, Photodegradation of dye pollutants catalyzed by porous K3PW12O40 under visible irradiation, Environ. Sci. Technol. 40 (2006)

S.F. Chen, S.J. Zhang, W. Liu, W. Zhao, Preparation and activity evaluation of p–n junction photocatalyst NiO/TiO2, J. Hazard. Mater. 155 (2008) 320

S.F. Chen, W. Zhao, W. Liu, S.J. Zhang, Preparation, characterization and activity evaluation of p–n junction photocatalyst p-ZnO/n-TiO2, Appl. Surf. Sci. 255 (2008)

APPENDIX A1

DATA OF XRD $CaFe_2O_4$ PHOTOCATALYST ANALYSIS

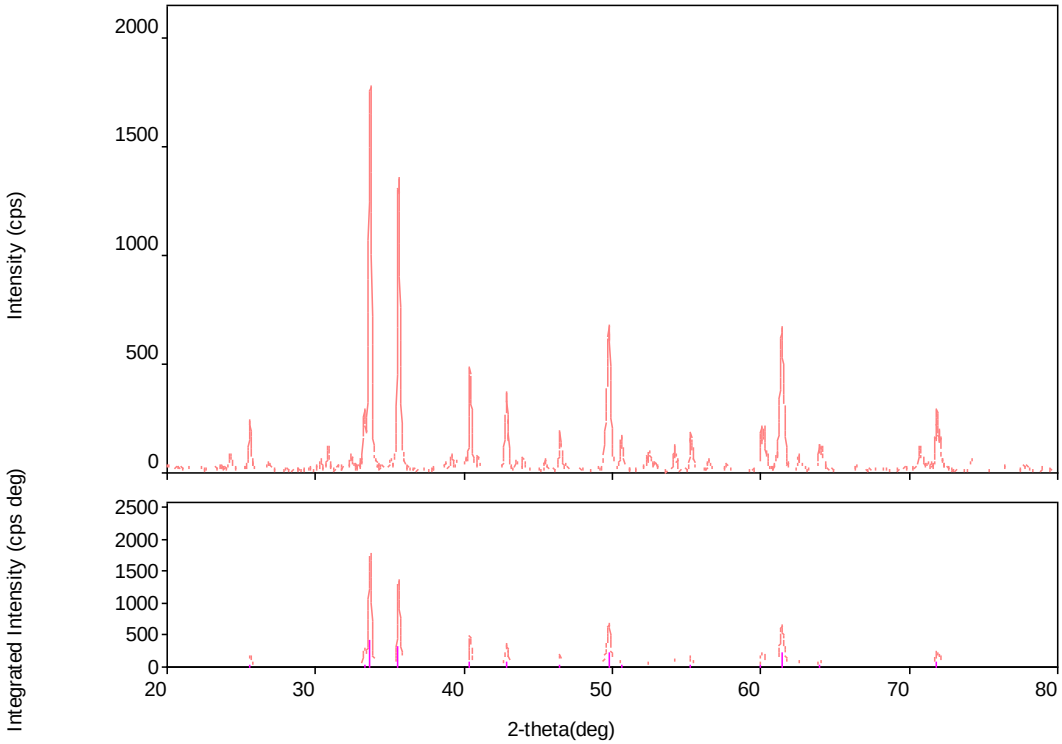

XG	Cu/30 kV/15 mA	Duration time / Scan speed	1 deg/min
Goniometer		Step / Sampling	0.02 deg
Attachment	-	Measurement axis	2ƒÆ/ƒÆ
K-beta filter	-	Scan range	20-80 deg
Incident	-	Incident slit	-
Receiving	-	Vertical divergence	-
Counter	-	Receiving slit #1	-
		Receiving slit #2	-

2-theta (deg)	d (ang.)	Height (cps)	Int. I(cps¥deg)	FWHM(deg)	Size	Phase name
24.24(2)	3.669(3)	47(7)	8.8(7)	0.164(15)	519(49)	Unknown,
25.574(10)	3.4803(13)	162(13)	30.1(8)	0.148(7)	575(26)	Unknown,
26.72(3)	3.334(4)	17(4)	4.9(5)	0.25(3)	345(40)	Unknown,
30.337(16)	2.9438(15)	40(6)	4.4(5)	0.076(18)	1136(273)	Unknown,
30.849(15)	2.8962(14)	92(10)	14.6(9)	0.12(2)	730(123)	Unknown,
32.35(3)	2.765(3)	42(6)	7.9(9)	0.15(3)	579(133)	Unknown,
33.289(10)	2.6892(8)	187(14)	33.6(16)	0.155(10)	558(35)	Unknown,
33.687(4)	2.6583(3)	1295(36)	298(3)	0.198(3)	439(8)	Unknown,
35.02(7)	2.560(5)	14(4)	3.8(9)	0.21(7)	411(140)	Unknown,
35.561(5)	2.5224(3)	1022(32)	223(3)	0.177(4)	492(10)	Unknown,
38.655(19)	2.3273(11)	22(5)	7.4(15)	0.23(5)	391(84)	Unknown,
39.187(12)	2.2970(7)	53(7)	10.1(11)	0.150(19)	586(74)	Unknown,
39.492(16)	2.2800(9)	37(6)	6.3(7)	0.13(2)	692(135)	Unknown,
40.054(11)	2.2492(6)	47(7)	7.2(7)	0.116(18)	760(119)	Unknown,
40.402(4)	2.2307(2)	422(21)	71.6(13)	0.130(5)	681(24)	Unknown,
40.930(9)	2.2031(4)	57(8)	9.4(6)	0.112(17)	789(118)	Unknown,
42.871(9)	2.1078(4)	252(16)	61.3(13)	0.201(9)	443(20)	Unknown,
43.489(17)	2.0792(8)	41(6)	7.0(5)	0.11(2)	836(153)	Unknown,
43.964(10)	2.0578(5)	46(7)	7.5(4)	0.130(12)	686(64)	Unknown,
45.415(19)	1.9954(8)	41(6)	6.1(6)	0.12(2)	760(138)	Unknown,
46.467(9)	1.9527(3)	129(11)	26.3(10)	0.139(12)	649(54)	Unknown,
49.785(8)	1.8300(3)	465(22)	158(2)	0.291(7)	315(8)	Unknown,
50.581(8)	1.8031(3)	144(12)	25.4(9)	0.143(9)	644(42)	Unknown,
52.50(3)	1.7416(9)	57(8)	19.1(10)	0.31(2)	294(21)	Unknown,
52.837(15)	1.7313(5)	37(6)	5.0(5)	0.127(16)	727(93)	Unknown,
54.184(11)	1.6914(3)	89(9)	14.6(8)	0.149(12)	627(49)	Unknown,
55.277(7)	1.6605(2)	155(12)	27.2(8)	0.137(8)	685(38)	Unknown,
56.533(5)	1.62653(13)	37(6)	7.8(3)	0.172(11)	547(36)	Unknown,
57.61(3)	1.5987(7)	16(4)	3.7(4)	0.22(3)	440(61)	Unknown,

60.008(11)	1.5404(3)	165(13)	28(3)	0.137(13)	697(67)	Unknown,
60.235(11)	1.5351(3)	140(12)	24(3)	0.139(18)	691(88)	Unknown,
61.419(6)	1.50833(13)	504(22)	163.1(18)	0.264(6)	365(8)	Unknown,
62.547(12)	1.4838(3)	57(8)	9.7(6)	0.140(11)	696(54)	Unknown,
63.904(14)	1.4555(3)	102(10)	27.0(11)	0.232(14)	421(25)	Unknown,
66.3(2)	1.408(5)	7(3)	4.1(7)	0.45(17)	222(85)	Unknown,
68.33(2)	1.3716(4)	21(5)	4.9(4)	0.18(2)	562(77)	Unknown,
69.757(15)	1.3470(3)	29(5)	4.4(5)	0.137(16)	741(85)	Unknown,
70.711(9)	1.33118(15)	104(10)	23.9(9)	0.156(11)	652(48)	Unknown,
71.280(18)	1.3219(3)	30(5)	5.8(7)	0.13(2)	781(148)	Unknown,
71.851(8)	1.31284(12)	255(16)	63.9(14)	0.170(8)	602(29)	Unknown,
74.25(2)	1.2763(4)	43(7)	10.9(8)	0.21(2)	491(57)	Unknown,
76.49(7)	1.2443(9)	13(4)	3.6(9)	0.25(7)	419(119)	Unknown,
77.64(3)	1.2288(4)	20(5)	6.9(8)	0.23(7)	466(145)	Unknown,
78.96(4)	1.2115(5)	14(4)	2.4(6)	0.16(4)	680(156)	Unknown,

APPENDIX A2

DATA OF XRD $CaFe_2O_4$-WO_3 PHOTOCATALYST ANALYSIS

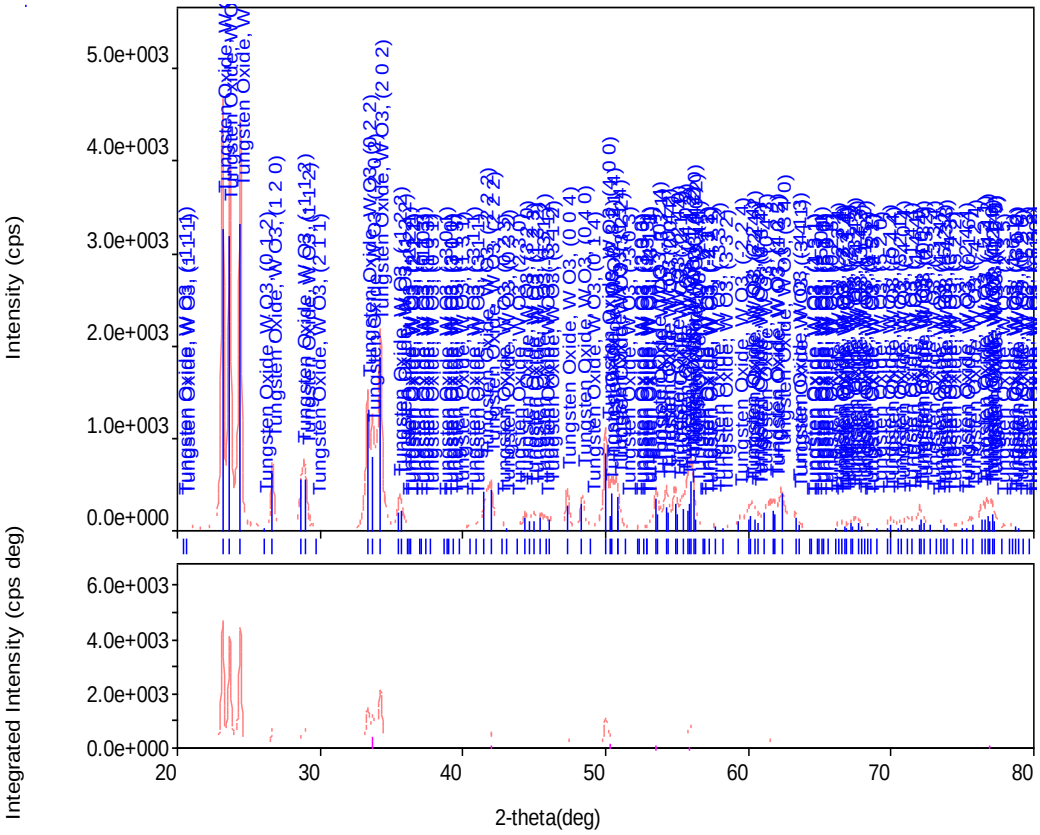

XG	Cu/30 kV/15 mA	Duration time / Scan speed	1 deg/min
Goniometer		Step / Sampling	0.02 deg
Attachment	-	Measurement axis	2ƒÆ/ƒÆ
K-beta filter	-	Scan range	20-80 deg
Incident	-	Incident slit	-
Receiving	-	Vertical divergence	-
Counter	-	Receiving slit #1	-
		Receiving slit #2	-

2-theta (deg)	d (ang.)	Height (cps)	Int. I(cps¥deg)	FWHM(deg)	Size	Phase name
23.177(3)	3.8346(6)	3249(57)	787(7)	0.185(3)	459(7)	Unknown,
23.665(4)	3.7566(6)	2787(53)	710(6)	0.193(4)	440(8)	Unknown,
24.402(4)	3.6447(5)	3182(56)	843(5)	0.178(3)	478(8)	Unknown,
26.656(6)	3.3414(7)	507(23)	150(2)	0.193(10)	442(22)	Unknown,
28.892(8)	3.0877(9)	488(22)	271(3)	0.481(7)	178(2)	Unknown,
33.359(6)	2.6837(5)	901(30)	276(23)	0.239(8)	363(12)	Unknown,
33.623(17)	2.6633(13)	726(27)	481(29)	0.46(4)	189(16)	Unknown,
34.231(8)	2.6173(6)	1351(37)	452(12)	0.252(7)	344(9)	Unknown,
35.514(15)	2.5257(10)	216(15)	99(2)	0.393(12)	222(7)	Unknown,
41.09(4)	2.195(2)	27(5)	3.5(13)	0.09(5)	1004(623)	Unknown,
41.47(3)	2.1757(14)	133(12)	64(24)	0.38(10)	235(65)	Unknown,
41.95(2)	2.1517(10)	285(17)	195(23)	0.48(6)	184(24)	Unknown,
44.33(3)	2.0417(11)	97(10)	25(2)	0.23(2)	382(35)	Unknown,
44.88(4)	2.0178(16)	83(9)	32(4)	0.36(4)	252(26)	Unknown,
45.86(4)	1.9771(17)	82(9)	84(5)	0.95(9)	95(9)	Unknown,
47.291(10)	1.9205(4)	335(18)	80.3(18)	0.209(9)	434(18)	Unknown,
48.323(12)	1.8819(5)	282(17)	80.0(18)	0.238(11)	381(17)	Unknown,
49.961(7)	1.8240(2)	805(28)	216(10)	0.209(8)	439(18)	Unknown,
50.33(2)	1.8113(7)	352(19)	266(14)	0.64(3)	144(7)	Unknown,
50.727(16)	1.7982(5)	163(13)	39(5)	0.20(2)	454(53)	Unknown,
53.49(3)	1.7115(7)	200(14)	88(7)	0.40(5)	230(31)	Unknown,
53.51(5)	1.7109(15)	110(10)	51(8)	0.43(4)	215(20)	Unknown,
54.20(3)	1.6910(7)	279(17)	113(7)	0.37(3)	252(18)	Unknown,
54.77(2)	1.6746(6)	255(16)	119(8)	0.43(3)	219(16)	Unknown,
55.924(15)	1.6428(4)	491(22)	365(10)	0.69(2)	137(4)	Unknown,
60.32(3)	1.5331(7)	138(12)	128(7)	0.87(3)	110(3)	Unknown,
61.63(5)	1.5037(12)	175(13)	238(33)	1.28(9)	75(6)	Unknown,
62.30(3)	1.4891(6)	195(14)	57(6)	0.27(3)	355(39)	Unknown,
63.30(5)	1.4680(11)	81(9)	94(30)	1.1(4)	90(32)	Unknown,
67.53(5)	1.3860(9)	62(8)	97(2)	1.47(4)	68(2)	Unknown,

69.87(4)	1.3452(6)	50(7)	11.4(13)	0.21(4)	471(85)	Unknown,
71.45(17)	1.319(3)	23(5)	22(4)	0.9(2)	110(25)	Unknown,
72.00(3)	1.3105(4)	123(11)	39(4)	0.30(5)	339(52)	Unknown,
76.94(3)	1.2382(4)	183(14)	221(4)	1.12(2)	94.3(17)	Unknown,
78.57(2)	1.2165(3)	64(8)	17.4(13)	0.25(2)	422(39)	Unknown,

APPENDIX A3

DATA OF XRD $CaFe_2O_4$-V_2O_5 PHOTOCATALYST ANALYSIS

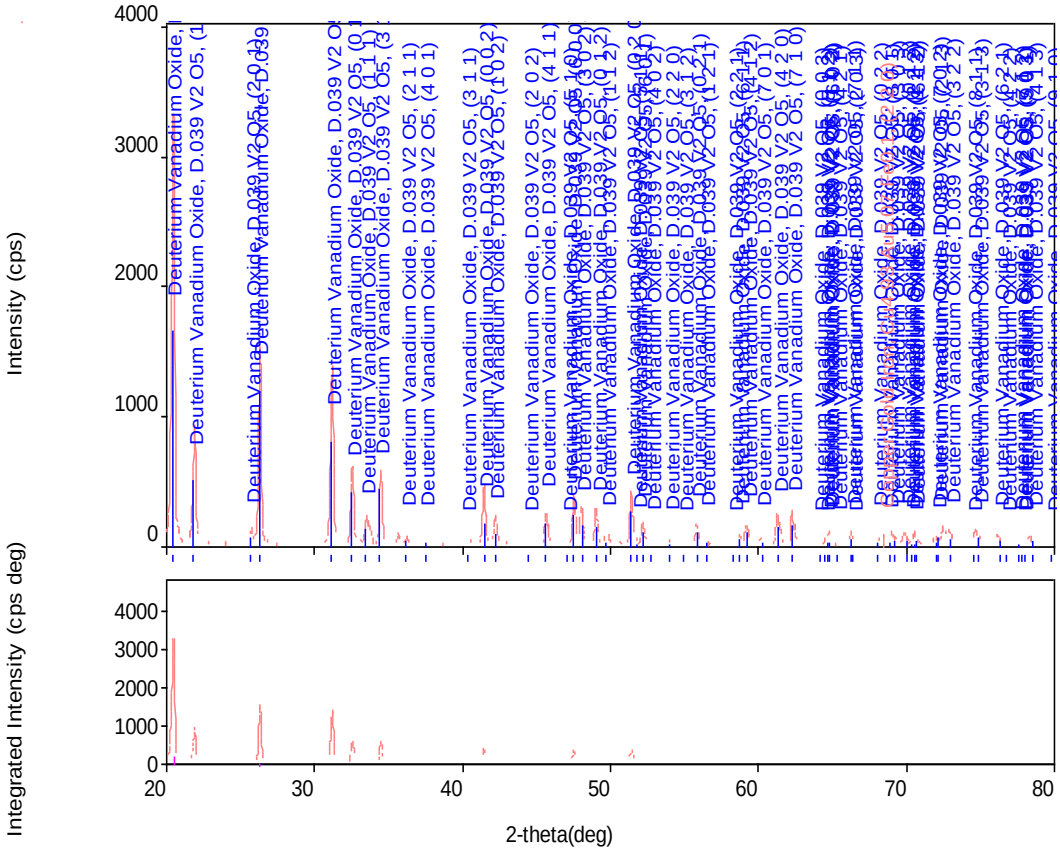

XG	Cu/30 kV/15 mA	Duration time / Scan speed	1 deg/min
Goniometer		Step / Sampling	0.02 deg
Attachment	-	Measurement axis	2ƒÆ/ƒÆ
K-beta filter	-	Scan range	20-80 deg
Incident	-	Incident slit	-
Receiving	-	Vertical divergence	-
Counter	-	Receiving slit #1	-
		Receiving slit #2	-

2-theta (deg)	d (ang.)	Height (cps)	Int. I(cps¥deg)	FWHM(deg)	Size	Phase name
20.479(4)	4.3332(8)	2206(47)	572(5)	0.214(3)	395(5)	Unknown,
21.922(8)	4.0512(14)	612(25)	155(2)	0.213(8)	398(14)	Unknown,
25.710(13)	3.4621(17)	81(9)	21.7(11)	0.212(14)	402(26)	Unknown,
26.324(4)	3.3828(5)	1081(33)	243(2)	0.179(3)	475(8)	Unknown,
31.184(5)	2.8658(4)	978(31)	241(2)	0.196(4)	440(8)	Unknown,
32.543(7)	2.7491(5)	458(21)	101.9(14)	0.182(5)	476(12)	Unknown,
33.509(13)	2.6721(10)	133(12)	53.0(17)	0.324(12)	268(10)	Unknown,
34.478(9)	2.5992(7)	418(20)	82(2)	0.179(6)	484(16)	Unknown,
35.60(2)	2.5196(15)	55(7)	10.8(8)	0.175(18)	497(50)	Unknown,
36.20(2)	2.4794(16)	46(7)	9.2(7)	0.17(2)	503(62)	Unknown,
37.55(2)	2.3933(12)	47(7)	8.9(5)	0.166(19)	529(59)	Unknown,
40.41(3)	2.2304(17)	29(5)	6.5(6)	0.17(4)	514(118)	Unknown,
41.419(7)	2.1782(4)	375(19)	87.6(12)	0.172(7)	517(21)	Unknown,
42.182(16)	2.1406(8)	169(13)	39.4(13)	0.175(15)	507(44)	Unknown,
45.631(14)	1.9865(6)	190(14)	44.5(14)	0.207(10)	435(21)	Unknown,
47.492(6)	1.9129(2)	338(18)	63.5(14)	0.145(7)	625(29)	Unknown,
48.013(8)	1.8933(3)	242(16)	54.1(14)	0.173(10)	524(29)	Unknown,
48.989(10)	1.8579(4)	206(14)	42.5(11)	0.186(8)	490(22)	Unknown,
49.74(2)	1.8316(8)	69(8)	19.6(9)	0.252(16)	363(23)	Unknown,
51.377(5)	1.77698(18)	343(19)	59(2)	0.155(6)	596(22)	Unknown,
51.719(18)	1.7660(6)	30(5)	16(2)	0.49(4)	189(17)	Unknown,
52.167(9)	1.7519(3)	159(13)	29.6(9)	0.165(10)	559(33)	Unknown,
52.69(3)	1.7359(9)	29(5)	6.2(7)	0.19(4)	478(92)	Unknown,
53.93(3)	1.6987(9)	28(5)	7.9(7)	0.27(3)	347(35)	Unknown,
55.33(2)	1.6589(7)	16(4)	2.9(5)	0.15(3)	640(148)	Unknown,
55.797(8)	1.6462(2)	150(12)	33.1(9)	0.183(9)	514(25)	Unknown,
56.416(15)	1.6296(4)	51(7)	11.6(6)	0.188(18)	502(49)	Unknown,
58.690(14)	1.5718(3)	70(8)	16.9(11)	0.17(2)	545(68)	Unknown,
59.144(11)	1.5608(3)	139(12)	34.5(13)	0.187(14)	511(38)	Unknown,
60.227(14)	1.5353(3)	59(8)	12.6(7)	0.200(14)	480(35)	Unknown,

61.256(6)	1.51196(14)	217(15)	55.8(12)	0.189(8)	511(21)	Unknown,
62.271(6)	1.48972(12)	252(16)	46.2(11)	0.152(5)	636(23)	Unknown,
64.73(3)	1.4389(6)	60(8)	25.5(14)	0.36(3)	272(23)	Unknown,
65.25(2)	1.4286(5)	24(5)	4.2(7)	0.14(3)	703(170)	Unknown,
66.211(10)	1.41030(19)	101(10)	19.0(9)	0.152(10)	651(41)	Unknown,
67.931(17)	1.3787(3)	51(7)	11.8(8)	0.18(2)	556(62)	Unknown,
68.490(17)	1.3688(3)	46(7)	10.1(9)	0.17(2)	598(84)	Unknown,
69.015(12)	1.3597(2)	88(9)	18.3(9)	0.166(15)	606(53)	Unknown,
69.825(18)	1.3459(3)	76(9)	19.1(10)	0.20(2)	505(51)	Unknown,
70.559(14)	1.3337(2)	68(8)	17.2(13)	0.22(2)	463(43)	Unknown,
71.917(15)	1.3118(2)	65(8)	15.5(8)	0.214(18)	480(41)	Unknown,
72.434(8)	1.30370(12)	124(11)	23.5(10)	0.170(8)	605(30)	Unknown,
72.820(12)	1.29774(18)	103(10)	26.0(12)	0.225(15)	458(30)	Unknown,
74.629(8)	1.27069(12)	113(11)	32.4(9)	0.220(11)	475(24)	Unknown,
76.137(12)	1.24924(16)	78(9)	15.7(7)	0.163(10)	648(39)	Unknown,
77.44(3)	1.2314(4)	20(5)	5.8(6)	0.26(4)	412(66)	Unknown,
78.325(12)	1.21972(15)	75(9)	16.2(8)	0.185(11)	580(36)	Unknown,

APPENDIX A4

DATA OF XRD CaO COMPOUND ANALYSIS

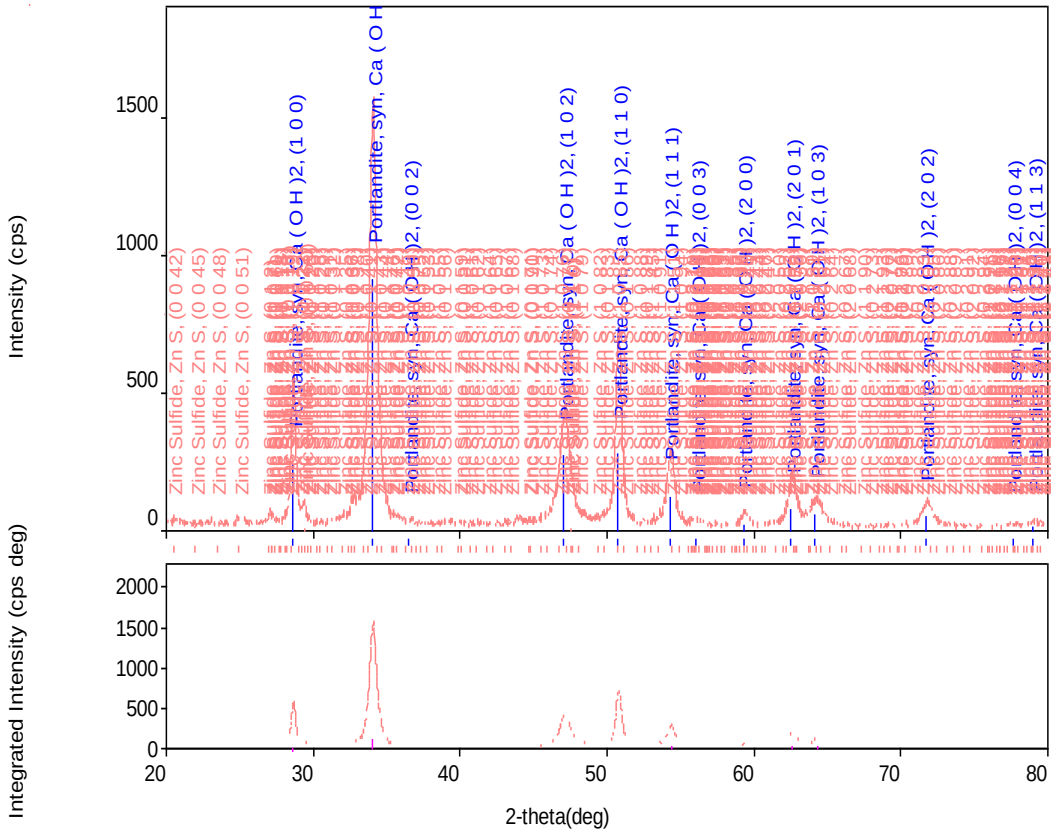

XG	Cu/30 kV/15 mA	Duration time / Scan speed	1 deg/min
Goniometer		Step / Sampling	0.02 deg
Attachment	-	Measurement axis	2ƒÆ/ƒÆ
K-beta filter	-	Scan range	20-80 deg
Incident	-	Incident slit	-
Receiving	-	Vertical divergence	-
Counter	-	Receiving slit #1	-
		Receiving slit #2	-

Phae name	**Formula**	**Space group**	**ICDD**
Portl	Ca	164 : P-	441481
Zinc	Zn	160 :	1089216

2-theta (deg)	d (ang.)	Height (cps)	Int. I(cps¥deg)	FWHM(deg)	Size	Phase name
28.647(13)	3.1136(14)	373(19)	166(4)	0.327(11)	262(9)	Portlandite, syn,
29.41(3)	3.035(3)	50(7)	17(3)	0.26(5)	334(64)	Zinc Sulfide,
34.030(8)	2.6323(6)	1025(32)	839(5)	0.585(8)	148(2)	Portlandite, syn,
47.063(17)	1.9293(7)	255(16)	256(4)	0.853(14)	106.1(17)	Portlandite, syn,
50.689(12)	1.7995(4)	485(22)	247(3)	0.413(12)	222(7)	Portlandite, syn,
54.39(2)	1.6853(7)	183(14)	129(3)	0.58(2)	161(6)	Portlandite, syn,
56.30(9)	1.633(2)	10(3)	7.5(11)	0.64(12)	147(27)	Portlandite, syn,
59.32(5)	1.5567(12)	30(6)	14.4(12)	0.45(4)	214(18)	Portlandite, syn,
62.61(2)	1.4825(5)	123(11)	98(2)	0.63(2)	155(5)	Portlandite, syn,
64.31(4)	1.4472(7)	62(8)	75(2)	0.96(5)	102(5)	Portlandite, syn,

APPENDIX A5

DATA OF Fe_2O_4 COMPOUND ANALYSIS

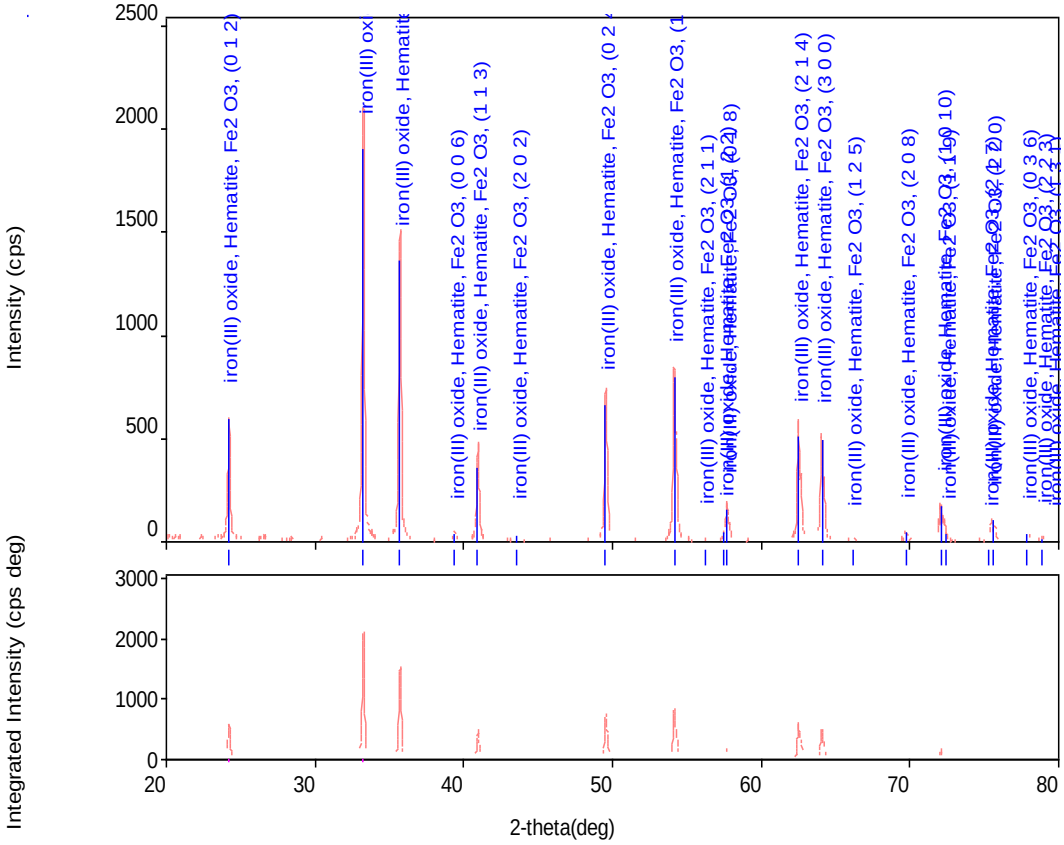

XG	Cu/30 kV/15 mA	Duration time / Scan speed	1 deg/min
Goniometer		Step / Sampling	0.02 deg
Attachment	-	Measurement axis	2ƒÆ/ƒÆ
K-beta filter	-	Scan range	20-80 deg
Incident	-	Incident slit	-
Receiving	-	Vertical divergence	-
Counter	-	Receiving slit #1	-
		Receiving slit #2	-

Phase name	Formula	Space group	ICDD
iron(III) oxide, Hematite	Fe2 O3	167 : R-3c,hexagonal	10790007 (ICDD)

2-theta (deg)	d (ang.)	Height (cps)	Int. I(cps¥deg)	FWHM(deg)	Size	Phase name
24.229(7)	3.6704(11)	407(20)	82.4(14)	0.156(6)	545(22)	iron(III) oxide,
33.231(5)	2.6938(4)	1708(41)	320(3)	0.138(4)	626(20)	iron(III) oxide,
35.692(4)	2.5135(3)	1245(35)	240(2)	0.143(4)	612(16)	iron(III) oxide,
39.400(13)	2.2851(7)	28(5)	5.7(4)	0.14(2)	623(107)	iron(III) oxide,
40.946(6)	2.2023(3)	369(19)	75.5(12)	0.152(7)	581(25)	iron(III) oxide,
43.54(4)	2.077(2)	25(5)	6.1(6)	0.21(3)	416(63)	iron(III) oxide,
49.530(4)	1.83883(13)	663(26)	137.7(14)	0.148(4)	619(18)	iron(III) oxide,
54.149(4)	1.69236(10)	803(28)	164.8(17)	0.143(4)	653(19)	iron(III) oxide,
57.715(12)	1.5960(3)	129(11)	38.4(10)	0.236(13)	402(22)	iron(III) oxide,
62.511(5)	1.48457(10)	539(23)	112.1(14)	0.144(4)	674(21)	iron(III) oxide,
64.052(5)	1.45254(10)	505(22)	111.1(14)	0.152(5)	642(21)	iron(III) oxide,
69.665(18)	1.3486(3)	47(7)	11.7(6)	0.177(19)	570(62)	iron(III) oxide,
72.061(10)	1.30953(16)	148(12)	45.0(14)	0.210(15)	490(34)	iron(III) oxide,
75.507(11)	1.25809(15)	110(10)	26.4(7)	0.172(10)	612(34)	iron(III) oxide,
77.821(16)	1.2263(2)	40(6)	8.0(5)	0.176(14)	607(48)	iron(III) oxide,
78.78(5)	1.2138(6)	14(4)	2.9(5)	0.17(4)	615(145)	iron(III) oxide,

APPENDIX A6

ANALYSIS OF WO_3 PHOTOCATALYST ANALYSIS

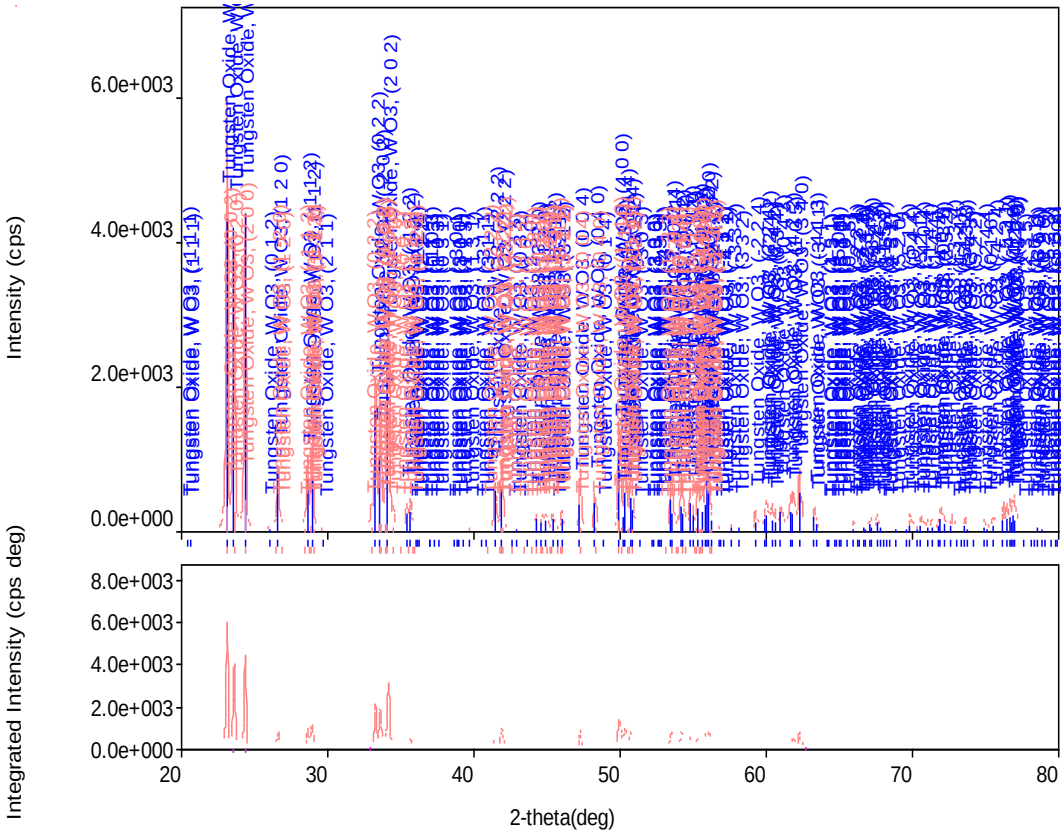

XG	Cu/30 kV/15 mA	Duration time / Scan speed	1 deg/min
Goniometer		Step / Sampling	0.02 deg
Attachment	-	Measurement axis	2ƒÆ/ƒÆ
K-beta filter	-	Scan range	20-80 deg
Incident	-	Incident slit	-
Receiving	-	Vertical divergence	-
Counter	-	Receiving slit #1	-
		Receiving slit #2	-

Phase name	**Formula**	**Space group**	**ICDD**
Tungsten Oxide	W O3	2 : P-1	201323 (ICDD)

2-theta (deg)	d (ang.)	Height (cps)	Int. I(cps¥deg)	FWHM(deg)	Size	Phase name
23.123(3)	3.8434(5)	4448(67)	739(7)	0.131(2)	645(12)	Tungsten Oxide,
23.592(4)	3.7680(6)	2815(53)	539(6)	0.151(3)	561(12)	Tungsten Oxide,
24.358(4)	3.6512(6)	3368(58)	585(6)	0.134(3)	631(13)	Tungsten Oxide,
26.592(8)	3.3493(9)	698(26)	137(3)	0.134(9)	636(41)	Tungsten Oxide,
26.770(13)	3.3274(15)	85(9)	12(2)	0.10(3)	842(216)	Tungsten Oxide,
28.606(6)	3.1179(6)	748(27)	134(4)	0.124(9)	689(50)	Tungsten Oxide,
28.900(6)	3.0869(7)	883(30)	199(5)	0.160(6)	535(21)	Tungsten Oxide,
32.952(19)	2.7160(15)	208(14)	122(23)	0.41(8)	211(43)	Tungsten Oxide,
33.252(4)	2.6921(3)	1656(41)	249(12)	0.114(5)	759(32)	Tungsten Oxide,
33.549(5)	2.6690(4)	1337(37)	252(8)	0.138(6)	627(29)	Tungsten Oxide,
34.167(3)	2.6221(2)	2332(48)	515(7)	0.176(3)	492(9)	Tungsten Oxide,
34.477(10)	2.5993(7)	215(15)	30(3)	0.107(17)	813(132)	Tungsten Oxide,
35.394(12)	2.5339(9)	272(16)	54(5)	0.151(18)	575(67)	Tungsten Oxide,
35.613(10)	2.5189(7)	292(17)	58(5)	0.143(15)	609(63)	Tungsten Oxide,
39.77(2)	2.2645(12)	46(7)	6.0(10)	0.10(2)	879(216)	Unknown,
40.92(3)	2.2034(15)	49(7)	15.3(11)	0.25(3)	351(41)	Tungsten Oxide,
41.426(5)	2.1779(2)	547(23)	95.1(17)	0.140(6)	635(26)	Tungsten Oxide,
41.882(5)	2.1552(2)	818(29)	158(2)	0.155(4)	572(16)	Tungsten Oxide,
42.965(13)	2.1034(6)	49(7)	6.3(6)	0.110(17)	810(123)	Tungsten Oxide,
44.267(10)	2.0445(4)	180(13)	32.5(15)	0.135(13)	665(63)	Tungsten Oxide,
44.665(13)	2.0271(5)	181(13)	42(5)	0.16(3)	558(89)	Tungsten Oxide,
44.887(13)	2.0176(6)	131(11)	24(4)	0.13(2)	715(133)	Tungsten Oxide,
45.357(12)	1.9978(5)	164(13)	34(2)	0.149(19)	602(75)	Tungsten Oxide,
46.013(7)	1.9709(3)	249(16)	36.3(17)	0.112(9)	803(67)	Tungsten Oxide,
47.252(4)	1.92201(17)	748(27)	108(2)	0.129(4)	704(23)	Tungsten Oxide,
48.234(6)	1.8852(2)	464(22)	85.5(19)	0.142(8)	641(34)	Tungsten Oxide,
49.919(3)	1.82540(12)	1319(36)	246(4)	0.144(4)	636(18)	Tungsten Oxide,
50.343(5)	1.81104(15)	832(29)	169(4)	0.158(7)	580(24)	Tungsten Oxide,
50.724(7)	1.7983(2)	702(26)	168(4)	0.184(9)	499(24)	Tungsten Oxide,
53.05(5)	1.7249(16)	52(7)	46(11)	0.59(16)	157(43)	Tungsten Oxide,

53.472(5)	1.71219(15)	733(27)	119(7)	0.126(5)	735(29)	Tungsten Oxide,
54.167(7)	1.6918(2)	623(25)	150(3)	0.158(9)	589(35)	Tungsten Oxide,
54.766(6)	1.67475(18)	466(22)	79(3)	0.138(9)	679(42)	Tungsten Oxide,
55.326(7)	1.6591(2)	479(22)	101(6)	0.161(11)	581(40)	Tungsten Oxide,
55.620(10)	1.6510(3)	327(18)	61(8)	0.139(18)	676(86)	Tungsten Oxide,
55.893(14)	1.6436(4)	600(24)	271(12)	0.366(17)	257(12)	Tungsten Oxide,
57.610(13)	1.5986(3)	73(9)	6.8(10)	0.080(15)	1182(227)	Tungsten Oxide,
58.154(12)	1.5850(3)	84(9)	10.9(11)	0.121(11)	783(68)	Tungsten Oxide,
59.222(5)	1.55894(12)	227(15)	36.2(11)	0.129(6)	740(32)	Tungsten Oxide,
59.948(13)	1.5418(3)	300(17)	82(4)	0.252(14)	380(22)	Tungsten Oxide,
60.405(10)	1.5312(2)	251(16)	40(3)	0.148(13)	648(57)	Tungsten Oxide,
60.558(16)	1.5277(4)	112(11)	14(3)	0.12(2)	805(150)	Tungsten Oxide,
60.969(6)	1.51838(14)	281(17)	41(2)	0.136(6)	710(33)	Tungsten Oxide,
61.651(11)	1.5032(3)	237(15)	29(3)	0.095(12)	1022(130)	Tungsten Oxide,
61.892(11)	1.4979(2)	247(16)	89(5)	0.336(15)	288(13)	Tungsten Oxide,
62.258(4)	1.49000(8)	723(27)	103(3)	0.133(3)	730(18)	Tungsten Oxide,
62.68(15)	1.481(3)	56(8)	112(15)	1.9(2)	52(6)	Tungsten Oxide,
63.269(6)	1.46860(12)	301(17)	49(3)	0.150(7)	651(30)	Tungsten Oxide,
65.982(10)	1.41464(18)	84(9)	12.9(10)	0.117(10)	844(75)	Tungsten Oxide,
66.249(19)	1.4096(4)	45(7)	10.0(16)	0.16(3)	628(119)	Tungsten Oxide,
66.635(9)	1.40235(17)	101(10)	17.7(13)	0.135(11)	736(62)	Tungsten Oxide,
67.091(8)	1.39392(14)	170(13)	34.9(13)	0.149(9)	668(42)	Tungsten Oxide,
67.576(8)	1.38510(14)	172(13)	31.2(14)	0.133(8)	748(47)	Tungsten Oxide,
68.90(16)	1.362(3)	12(3)	2.5(18)	0.16(15)	610(552)	Tungsten Oxide,
69.569(18)	1.3502(3)	40(6)	3.2(12)	0.07(3)	1353(508)	Tungsten Oxide,
69.826(10)	1.34586(17)	161(13)	19.2(11)	0.112(7)	900(60)	Tungsten Oxide,
70.575(11)	1.33341(19)	127(11)	24.1(19)	0.178(13)	570(42)	Tungsten Oxide,
71.019(12)	1.32616(19)	95(10)	11.2(11)	0.101(10)	1013(104)	Tungsten Oxide,
71.335(12)	1.32105(19)	98(10)	11.8(10)	0.102(11)	1002(110)	Tungsten Oxide,
71.983(8)	1.31075(12)	245(16)	58.4(15)	0.215(8)	476(19)	Tungsten Oxide,
72.643(10)	1.30045(16)	162(13)	20.3(15)	0.117(8)	879(61)	Tungsten Oxide,
73.57(2)	1.2864(4)	123(11)	21(2)	0.12(2)	832(157)	Tungsten Oxide,

74.86(6)	1.2673(8)	48(7)	11(3)	0.19(6)	555(162)	Tungsten Oxide,
75.504(13)	1.25812(18)	161(13)	35(2)	0.175(16)	601(54)	Tungsten Oxide,
76.219(10)	1.24810(13)	310(18)	53(3)	0.140(10)	753(55)	Tungsten Oxide,
76.42(2)	1.2453(3)	150(12)	24(8)	0.13(4)	820(278)	Tungsten Oxide,
76.689(17)	1.2416(2)	304(17)	65(17)	0.18(3)	601(99)	Tungsten Oxide,
76.94(3)	1.2381(4)	237(15)	86(18)	0.30(7)	356(87)	Tungsten Oxide,
78.47(10)	1.2178(13)	33(6)	25(5)	0.66(10)	162(24)	Tungsten Oxide,

APPENDIX A7

DATA OF XRD V_2O_5 PHOTOCATALYST ANALYSIS

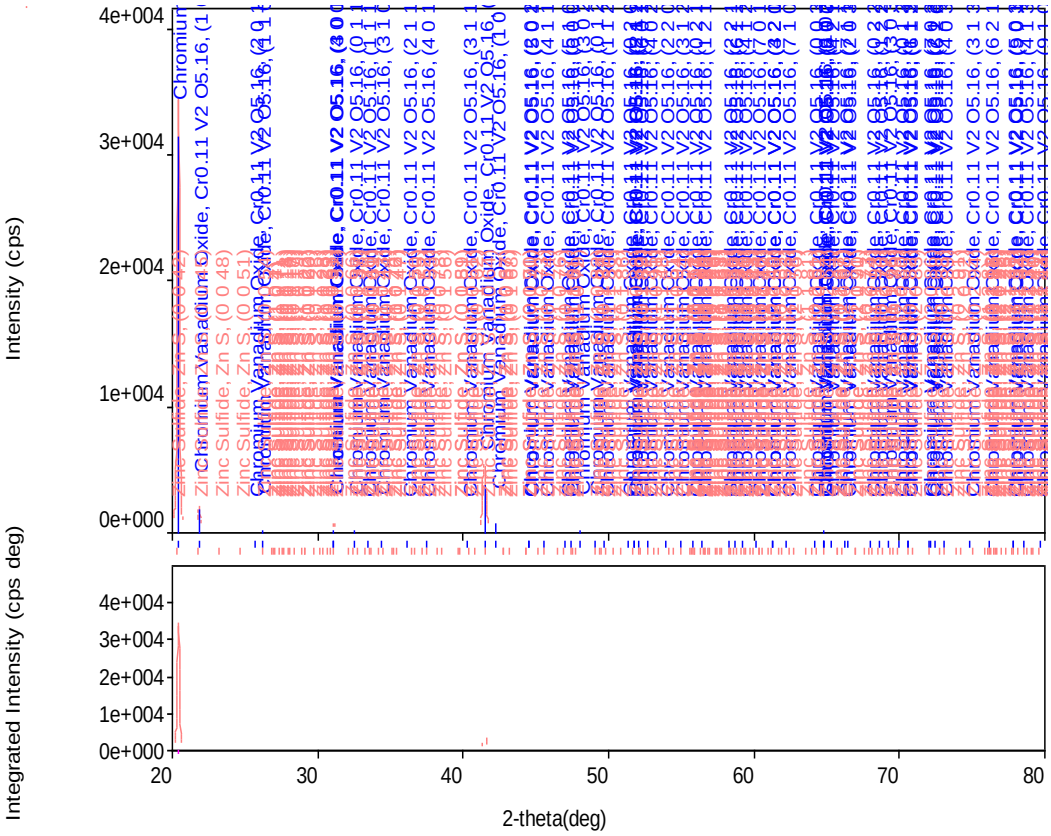

XG	Cu/30 kV/15 mA	Duration time / Scan speed	1 deg/min
Goniometer		Step / Sampling	0.02 deg
Attachment	-	Measurement axis	2ƒÆ/ƒÆ
K-beta filter	-	Scan range	20-80 deg
Incident	-	Incident slit	-
Receiving	-	Vertical divergence	-
Counter	-	Receiving slit #1	-
		Receiving slit #2	-

Phase name	**Formula**	**Space group**	**ICDD**
Chromium Vanadium	Cr0.11 V2	59 : Pmmn,choice-	10891323 (ICDD)
Zinc Sulfide	Zn S	160 :	10892140 (ICDD)

2-theta (deg)	d (ang.)	Height (cps)	Int. I(cps¥deg)	FWHM(deg)	Size	Phase name
20.429(2)	4.3437(5)	24489(156)	5200(32)	0.1725(16)	489(5)	Chromium
21.846(5)	4.0650(9)	1388(37)	322(7)	0.190(5)	444(11)	Chromium
25.653(13)	3.4697(17)	176(13)	35.3(13)	0.164(13)	519(42)	Chromium
26.219(15)	3.3961(18)	313(18)	75.0(18)	0.156(14)	546(48)	Chromium
28.61(6)	3.118(6)	28(5)	12.3(11)	0.42(6)	206(28)	Zinc Sulfide,
29.06(3)	3.071(3)	54(7)	11.3(12)	0.20(2)	439(46)	Zinc Sulfide,
31.092(9)	2.8741(8)	683(26)	151(2)	0.159(8)	540(27)	Chromium
32.473(15)	2.7549(12)	162(13)	38.1(12)	0.193(12)	448(28)	Chromium
33.40(2)	2.6804(19)	49(7)	9.4(8)	0.182(16)	476(43)	Chromium
34.416(15)	2.6037(11)	91(10)	18.3(10)	0.189(12)	460(29)	Chromium
41.428(3)	2.17774(15)	4251(65)	1255(6)	0.241(2)	368(3)	Chromium
42.167(6)	2.1413(3)	690(26)	205(3)	0.242(5)	367(8)	Chromium
44.62(16)	2.029(7)	10(3)	6.5(19)	0.60(14)	151(35)	Chromium
45.53(4)	1.9905(15)	59(8)	14.6(15)	0.22(3)	415(60)	Chromium
47.411(7)	1.9159(3)	207(14)	39.2(12)	0.149(9)	607(37)	Chromium
47.967(10)	1.8950(4)	268(16)	77.0(16)	0.226(10)	402(17)	Chromium
48.93(2)	1.8599(7)	106(10)	38.1(15)	0.296(15)	308(16)	Chromium
49.65(4)	1.8348(12)	27(5)	7.0(9)	0.21(4)	434(87)	Chromium
51.277(18)	1.7802(6)	75(9)	25.9(10)	0.22(3)	411(53)	Chromium
52.083(15)	1.7545(5)	81(9)	15.5(10)	0.171(16)	541(52)	Chromium
52.691(16)	1.7357(5)	26(5)	4.0(7)	0.13(3)	690(137)	Chromium
58.59(4)	1.5743(10)	21(5)	5.0(9)	0.22(5)	437(107)	Chromium
59.09(3)	1.5621(7)	51(7)	13.0(8)	0.24(3)	396(45)	Chromium
60.25(4)	1.5347(10)	21(5)	8.5(11)	0.39(5)	248(32)	Chromium
61.25(3)	1.5120(6)	40(6)	12.9(8)	0.25(3)	388(45)	Chromium
62.192(17)	1.4914(4)	66(8)	17.3(9)	0.22(2)	449(41)	Chromium
64.548(13)	1.4426(3)	235(15)	130(3)	0.415(14)	236(8)	Chromium
66.15(3)	1.4115(5)	28(5)	4.9(8)	0.16(3)	601(96)	Chromium
69.01(3)	1.3597(4)	119(11)	53(3)	0.34(3)	295(29)	Chromium
69.84(4)	1.3457(6)	66(8)	30(4)	0.34(6)	297(49)	Chromium

70.50(3)	1.3346(5)	42(6)	23(5)	0.37(10)	273(70)	Chromium
72.07(10)	1.3094(16)	18(4)	12(3)	0.59(14)	173(42)	Chromium
72.83(6)	1.2976(10)	47(7)	23(3)	0.45(8)	230(39)	Chromium
74.72(3)	1.2694(4)	58(8)	24.9(12)	0.40(3)	264(18)	Chromium
76.15(4)	1.2490(6)	11(3)	2.3(4)	0.20(4)	537(115)	Chromium
78.38(5)	1.2190(6)	34(6)	16.0(9)	0.38(5)	283(35)	Chromium

APPENDIX B1

DATA OF BET $CaFe_2O_4$ PHOTOCATALYST ANALYSIS

Sample:	CaFe04		
Operator:	Shaharunizam		
Submitter:	UMP		
File:	C:\2020\DATA\000-076.SMP		
Started:	12/9/2011 4:11:51PM	Analysis Adsorptive:	N2
Completed:	12/9/2011 7:23:14PM	Analysis Bath Temp.:	-195.871 °C
Report Time:	12/13/2011 9:24:56AM	Thermal Correction:	No
Sample Mass:	0.1635 g	Warm Free Space:	26.6824 cm³ Measured
Cold Free Space:	81.2935 cm³	Equilibration Interval:	5 s
Low Pressure Dose:	None	Automatic Degas:	Yes

Summary Report

Surface Area

Single point surface area at P/Po = 0.300114832:	2.4117 m²/g
BET Surface Area:	2.7560 m²/g
Langmuir Surface Area:	4.9457 m²/g
t-Plot External Surface Area:	4.1239 m²/g
BJH Adsorption cumulative surface area of pores between 17.000 Å and 3000.000 Å diameter:	3.528 m²/g
BJH Desorption cumulative surface area of pores between 17.000 Å and 3000.000 Å diameter:	6.1116 m²/g

Pore Volume

Single point adsorption total pore volume of pores less than 1230.575 Å diameter at P/Po = 0.984013979:	0.007777 cm^3/g
Single point desorption total pore volume of pores less than 689.972 Å diameter at P/Po = 0.971136105:	0.007294 cm^3/g
t-Plot micropore volume:	-0.000753 cm^3/g
BJH Adsorption cumulative volume of pores between 17.000 Å and 3000.000 Å diameter:	0.008477 cm^3/g
BJH Desorption cumulative volume of pores between 17.000 Å and 3000.000 Å diameter:	0.008121 cm^3/g

Pore Size

Adsorption average pore width (4V/A by BET):	112.8740 Å
Desorption average pore width (4V/A by BET):	105.8673 Å
BJH Adsorption average pore diameter (4V/A):	96.117 Å
BJH Desorption average pore diameter (4V/A):	53.154 Å

BET Surface Area Report

BET Surface Area:	2.7560 ± 0.0832 m^2/g
Slope:	1.505239 ± 0.046964 g/cm^3 STP
Y-Intercept:	0.074284 ± 0.008216 g/cm^3 STP
C:	21.263404
Qm:	0.6331 cm^3/g STP
Correlation Coefficient:	0.9961288
Molecular Cross-Sectional Area:	0.1620 nm^2

Relative Pressure (P/Po)	Quantity Adsorbed (cm^3/g STP)	1/[Q(Po/P - 1)]
0.06904	0.390091	0.19011
0.080031	0.440201	0.197622
0.100244	0.480801	0.231723
0.120129	0.537338	0.254087
0.140077	0.581217	0.280266
0.160093	0.619786	0.307538
0.180167	0.654173	0.335936
0.200092	0.696261	0.359267
0.250131	0.736117	0.453144
0.300115	0.791583	0.541707

APPENDIX B2

DATA OF BET $CaFe_2O_4$-WO_3 PHOTOCATALYST ANALYSIS

Sample:	CaFe2O4-WO3		
Operator:	Shaharunizam		
Submitter:	UMP		
File:	C:\2020\DATA\000-075.SMP		
Started:	12/9/2011 7:58:02AM	Analysis Adsorptive:	N2
Completed:	12/9/2011 11:27:01AM	Analysis Bath Temp.:	-195.831 °C
Report Time:	12/13/2011 9:22:52AM	Thermal Correction:	No
Sample Mass:	0.5759 g	Warm Free Space:	27.2397 cm³ Measured
Cold Free Space:	82.2642 cm³	Equilibration Interval:	5 s
Low Pressure Dose:	None	Automatic Degas:	Yes

Summary Report

Surface Area

Single point surface area at P/Po = 0.300178917:	2.2862 m²/g
BET Surface Area:	2.3159 m²/g
Langmuir Surface Area:	3.5976 m²/g
t-Plot Micropore Area:	0.4824 m²/g
t-Plot External Surface Area:	1.8335 m²/g
BJH Adsorption cumulative surface area of pores between 17.000 Å and 3000.000 Å diameter:	1.520 m²/g
BJH Desorption cumulative surface area of pores between 17.000 Å and	2.0410 m²/g

3000.000 Å diameter:

Pore Volume

Single point adsorption total pore volume of pores less than 1238.025 Å diameter at P/Po = 0.984111933:	0.010813 cm^3/g
Single point desorption total pore volume of pores less than 779.397 Å diameter at P/Po = 0.974521188:	0.013922 cm^3/g
t-Plot micropore volume:	0.000267 cm^3/g
BJH Adsorption cumulative volume of pores between 17.000 Å and 3000.000 Å diameter:	0.015094 cm^3/g
BJH Desorption cumulative volume of pores between 17.000 Å and 3000.000 Å diameter:	0.015240 cm^3/g

Pore Size

Adsorption average pore width (4V/A by BET):	186.7518 Å
Desorption average pore width (4V/A by BET):	240.4644 Å
BJH Adsorption average pore diameter (4V/A):	397.099 Å
BJH Desorption average pore diameter (4V/A):	298.668 Å

Langmuir Surface Area Report

Langmuir Surface Area:	3.5976 ± 0.0632 m^2/g
Slope:	1.210041 ± 0.021264 g/cm^3 STP
Y-Intercept:	33.081009 ± 2.816345 $mmHg \cdot g/cm^3$ STP
b:	0.036578 1/mmHg
Qm:	0.8264 cm^3/g STP
Correlation Coefficient:	0.998767
Molecular Cross-Sectional Area:	0.1620 nm^2

Pressure (mmHg)	Quantity Adsorbed (cm^3/g STP)	P/Q ($mmHg \cdot g/cm^3$ STP)
52.09212	0.574175	90.72514
60.69256	0.582931	104.1162
75.79191	0.609877	124.274
90.95986	0.626531	145.1802
106.1171	0.646596	164.1165
121.2254	0.664698	182.3765
136.4252	0.6754	201.9917
151.5051	0.690793	219.3205
189.3184	0.723418	261.6998
227.2612	0.750433	302.84

APPENDIX B2

DATA OF BET $CaFe_2O_4$-V_2O_5 PHOTOCATALYST ANALYSIS

Sample:	CaFe2O4-V2O5		
Operator:	Shaharunizam		
Submitter:	UMP		
File:	C:\2020\DATA\000-073.SMP		
Started:	12/8/2011 5:47:23PM	Analysis Adsorptive:	N2
Completed:	12/8/2011 8:49:24PM	Analysis Bath Temp.:	-195.857 °C
Report Time:	12/13/2011 9:24:12AM	Thermal Correction:	No
Sample Mass:	0.2884 g	Warm Free Space:	27.1205 cm³ Measured
Cold Free Space:	83.6602 cm³	Equilibration Interval:	5 s
Low Pressure Dose:	None	Automatic Degas:	Yes

Summary Report

Surface Area

Single point surface area at P/Po = 0.319870519:	1.8928 m²/g
BET Surface Area:	1.8764 m²/g
Langmuir Surface Area:	2.6394 m²/g
t-Plot Micropore Area:	5.3519 m²/g
t-Plot External Surface Area:	-3.4755 m²/g
BJH Adsorption cumulative surface area of pores between 17.000 Å and 3000.000 Å diameter:	0.455 m²/g
BJH Desorption cumulative surface area of pores	

between 17.000 Å and 3000.000 Å diameter:	0.6467 m^2/g

Pore Volume

Single point adsorption total pore volume of pores less than 1245.539 Å diameter at P/Po = 0.984209537:	0.005140 cm^3/g
Single point desorption total pore volume of pores less than 769.075 Å diameter at P/Po = 0.974171323:	0.005179 cm^3/g
t-Plot micropore volume:	0.002861 cm^3/g
BJH Adsorption cumulative volume of pores between 17.000 Å and 3000.000 Å diameter:	0.007925 cm^3/g
BJH Desorption cumulative volume of pores between 17.000 Å and 3000.000 Å diameter:	0.007926 cm^3/g

Pore Size

Adsorption average pore width (4V/A by BET):	109.5601 Å
Desorption average pore width (4V/A by BET):	110.4056 Å
BJH Adsorption average pore diameter (4V/A):	696.580 Å
BJH Desorption average pore diameter (4V/A):	490.269 Å

BET Surface Area Report

BET Surface Area:	1.8764 ± 0.1900 m^2/g
Slope:	2.479815 ± 0.230694 g/cm^3 STP
Y-Intercept:	-0.159867 ± 0.044063 g/cm^3 STP
C:	-14.511716
Qm:	0.4310 cm^3/g STP
Correlation Coefficient:	0.9670824
Molecular Cross-Sectional Area:	0.1620 nm^2

Relative Pressure (P/Po)	Quantity Adsorbed (cm^3/g STP)	1/[Q(Po/P - 1)]
0.06909	1.046745	0.070903
0.080235	1.035158	0.084272
0.115123	1.005114	0.129439
0.138052	0.969255	0.165244
0.159823	0.938512	0.202688
0.179899	0.906228	0.242061
0.19985	0.87436	0.285654
0.219838	0.840605	0.335216
0.269817	0.748278	0.493827
0.319871	0.6393	0.735662

APPENDIX C

DATA OF SEM $CaFe_2O_4$ PHOTOCATALYST ANALYSIS

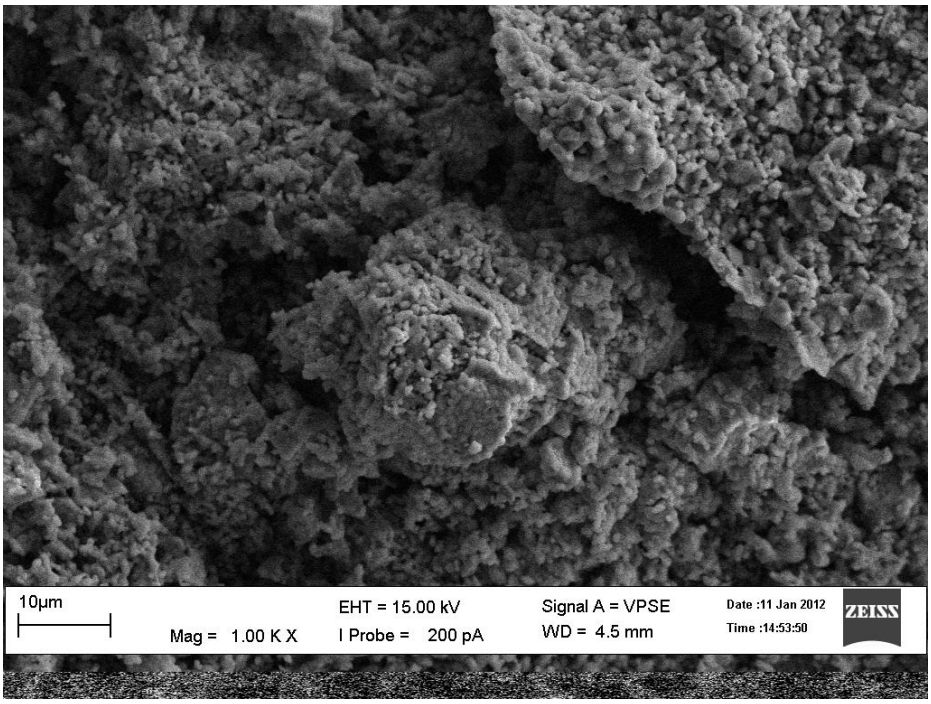

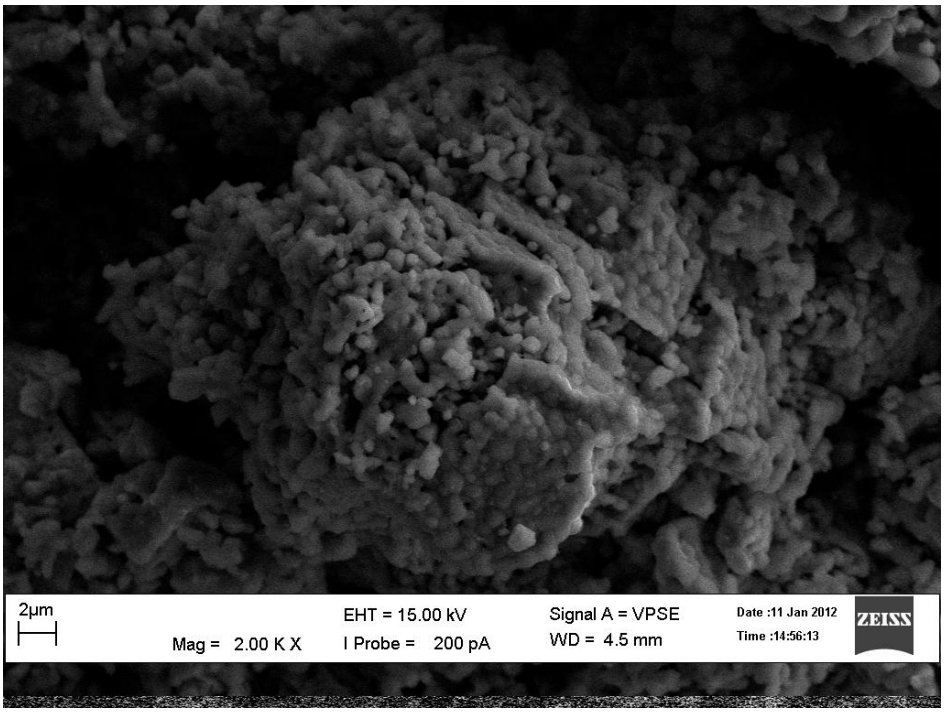

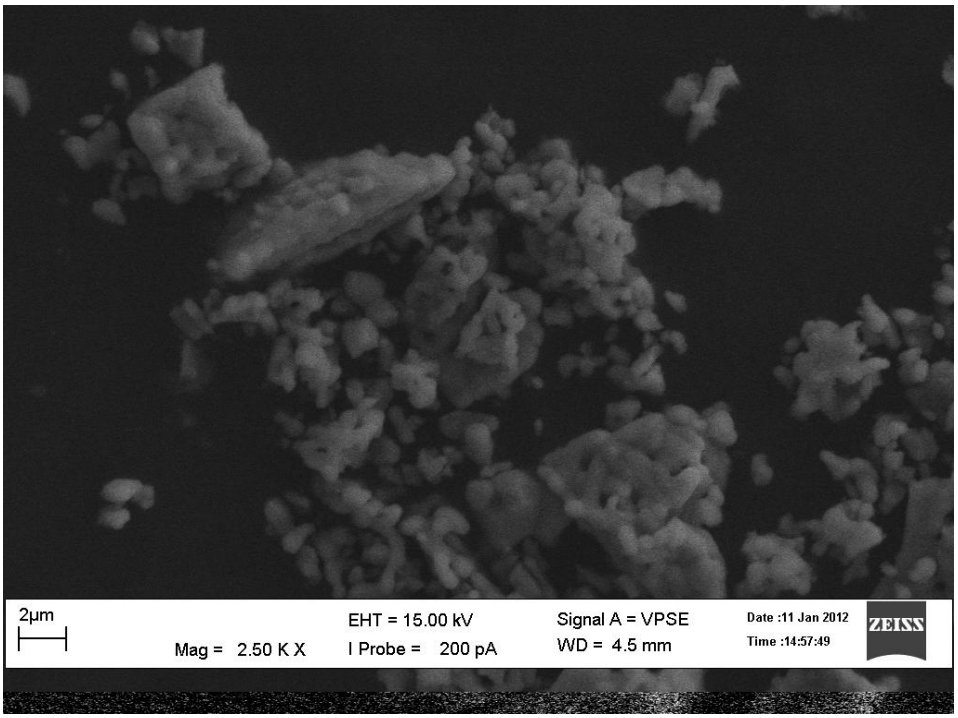
2µm
Mag = 2.50 K X
EHT = 15.00 kV
I Probe = 200 pA
Signal A = VPSE
WD = 4.5 mm
Date :11 Jan 2012
Time :14:57:49
ZEISS

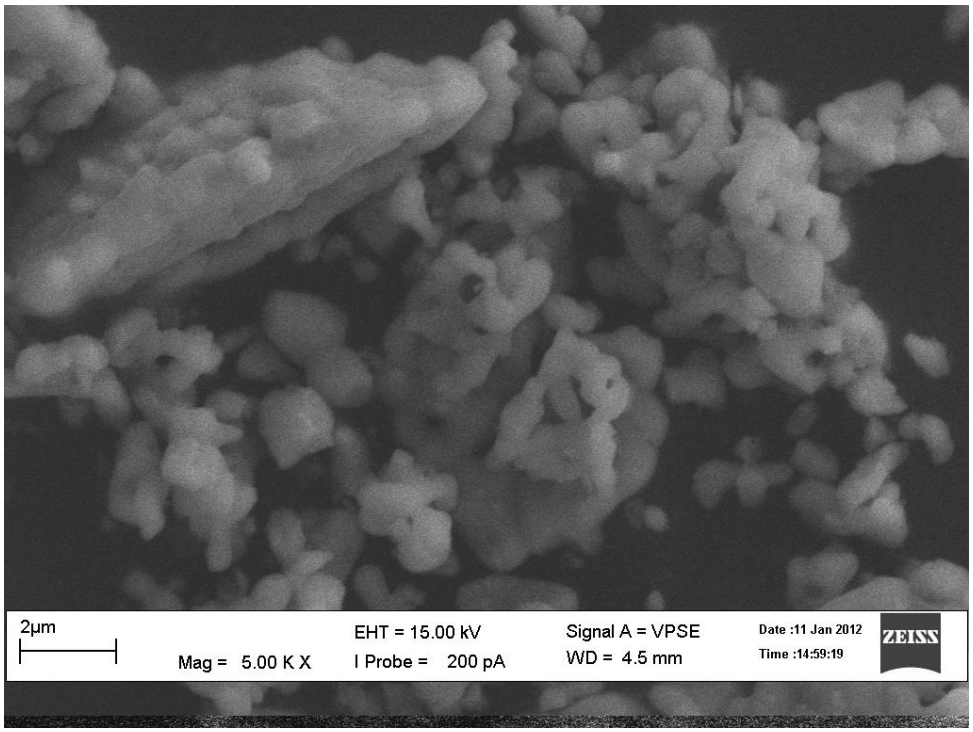
2µm
Mag = 5.00 K X
EHT = 15.00 kV
I Probe = 200 pA
Signal A = VPSE
WD = 4.5 mm
Date :11 Jan 2012
Time :14:59:19
ZEISS

APPENDIX D

DATA OF ADSORPTION DYE ONTO CATALYST
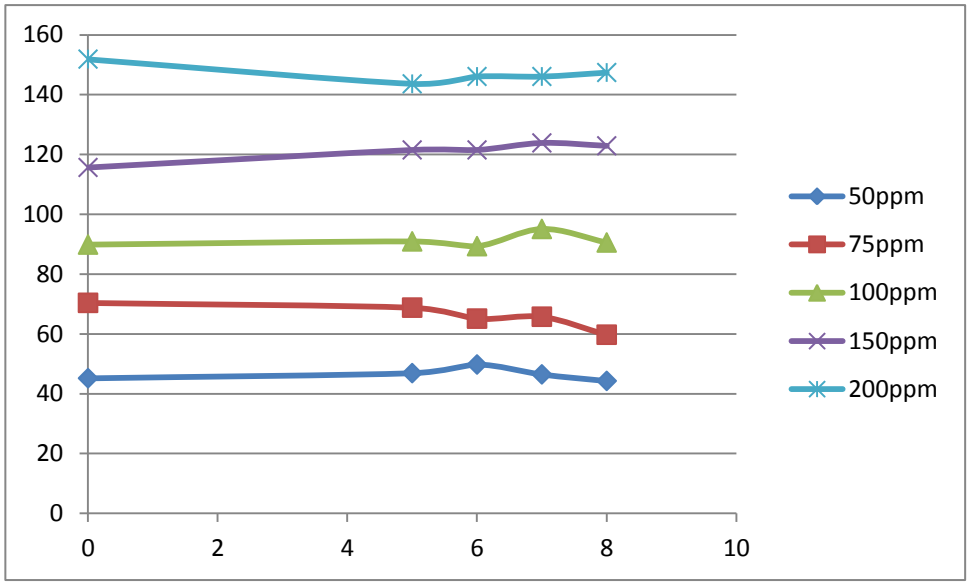
Time (h)	50 ppm	75 ppm	100 ppm	150 ppm	200ppm
0	45.14962	70.3468	89.84399	115.6272	151.8514
5	46.85429	68.74867	90.90941	121.487	143.5944
6	49.73093	65.07298	89.31128	121.487	146.0449
7	46.42813	65.71223	95.06455	123.8309	146.0449
8	44.24401	59.6926	90.53651	122.872	147.3767